CLASS VI PERMIT APPLICATION NARRATIVE
40 CFR 146.82(a)

BAYOU BEND EAST SL20220050 (BBE)

PBI CROSSWALK FOR BAYOU BEND EAST CLASS VI APPLICATION

Plan Number	Plan Document Title	Contains PBI
00	Narrative	Yes
	Appendix 1: Analytical Results	Yes
	Appendix 2: Copies of references used in support of this application for BBE-P1	Yes
	Appendix 3: Narrative Figures	Yes
03	Area of Review (AOR) and Corrective Action	Yes
	Appendix 3-1: Model Comparison Outputs	Yes
	Appendix 3-2: Artificial Penetrations – Wellbore Diagrams and Well Records	Yes
	Appendix 3-3: Copies of references used in support of the AOR and Corrective Action Plan	Yes
	Appendix 3-4 AOR and Corrective Action Plan Figures	Yes
	Appendix 3-5: Supplemental Model Output Figures	Yes
04	Financial Responsibility	Yes
05	Injection Well Construction	Yes
	Injection Well Construction Figures	Yes
06	Pre-Operational Logging and Testing Plan	Yes
07	Testing and Monitoring Plan	Yes
	Appendix 7-1: Quality Assurance and Surveillance Plan	Yes
	Appendix 7-2: Testing and Monitoring Plan Figures	Yes
08	Well Plugging Plan	Yes
	Well Plugging Plan Figures	Yes
09	Post Injection Site Care and Site Closure Plan	Yes
	Post-Injection Site Care and Site Closure Plan Figures	Yes
10	Emergency and Remedial Response Plan	Yes
	Emergency and Remedial Response Plan Figures	Yes

TABLE OF CONTENTS

LIST OF TABLES

LIST OF FIGURES


Claimed as PBI

Claimed as PBI

61

Figure 2-34: Typical pressure vs rate curve for a step-rate test (SRT). The injection rate is increased in discrete steps and at each step, the bottomhole pressure is recorded after it stabilizes. The injection rates and corresponding stabilized pressures are plotted, and they usually align with a straight line. A change of slope is usually observed at certain pressure, which corresponds to the pressure at which a fracture created at the wellbore starts propagating. This is known as the fracture propagation pressure (FPP). Once the fracture begins propagating, the subsequent points in the pressure vs rate plot align with a different straight line with a shallower slope. 64

Claimed as PBI

LIST OF APPENDICIES

1 PROJECT BACKGROUND AND CONTACT INFORMATION

GSDT Submission - Project Background and Contact Information

GSDT Module: Project Information Tracking
Tab(s): General Information tab; Facility Information and Owner/Operator Information tab

Please use the checkbox(es) to verify the following information was submitted to the GSDT:
☒ Required project and facility details ***[40 CFR 146.82(a)(1)]***

Bayou Bend East SL20220050 (BBE) is a Bayou Bend CCS LLC (Operator) proposed Texas State Waters carbon transport and sequestration (CCS) project. Operator is a joint venture between Chevron U.S.A. Inc. (Chevron), through its Chevron New Energies division, TotalEnergies, and Equinor. The project objective is to develop a CCS facility in Southeast Texas to reduce emissions from regional industrial facilities by transporting and sequestering carbon dioxide (CO_2) from industrial sources in the Beaumont/Port Arthur areas to support local, regional, and national lower carbon aspirations.

The Bayou Bend East SL20220050 Phase 1 (BBE-P1) project site is located on the Jefferson County Lease, High Island Block, Jefferson County (SL20220050, General Land Office, April 1, 2022; 40,865 acres) in Texas State Waters (**Figure 1-1**). Claimed as PBI [redacted]

Neither an injection depth waiver nor aquifer exemption expansion will be requested as part of this permit application.

Additionally, the Operator sought to conduct a balanced review of environmental, social, economic, and other factors in the vicinity of the BBE project area. Communities potentially adversely and disproportionately affected by human health, environmental, climate-related, and/or other cumulative harms or risks were identified and are being engaged. They will continue to proactively be engage through the permitting process and during project operations to promote the just treatment and meaningful involvement of the affected community in Underground Injection Control (UIC) permitting actions.

No federally recognized Native American tribal lands or territories are located within Jefferson or Chambers County (Texas Historical Commission, 2023).

Key project and facility details required by 40 CFR 146.82(a)(1) have been submitted directly in the Project Information Tracking module of the GSDT.

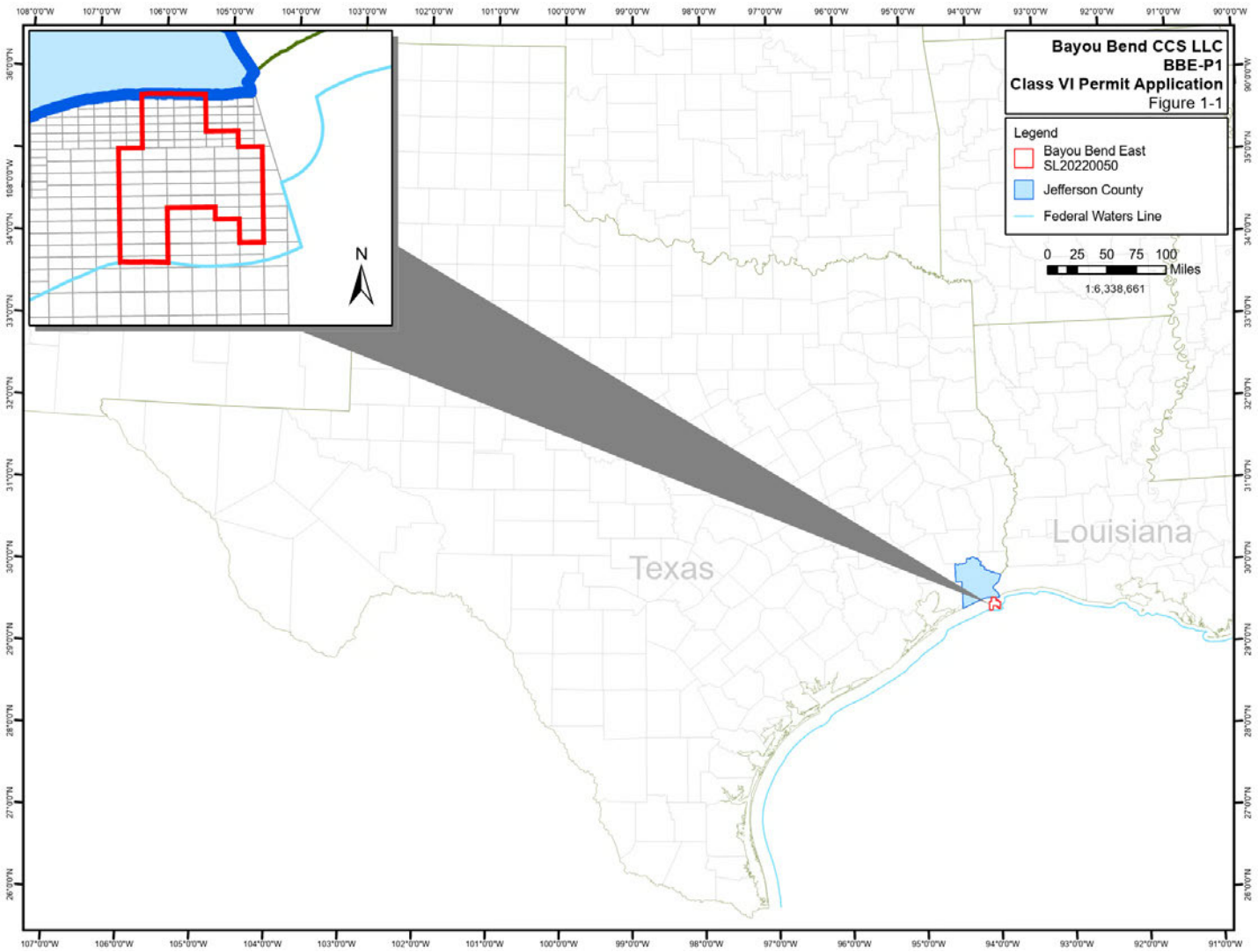

Figure 1-1: Location of the proposed BBE-P1; Jefferson County Lease, High Island Block (SL20220050), Texas.

2 SITE CHARACTERIZATION

Detailed site characterization information required per 40 CFR 146.82(a)(2), (3), (5), and (6), is provided in the following sections. Geologic and hydrogeologic data described in the site characterization sections below were used to develop a conceptual model of the proposed BBE-P1 geologic sequestration site.

2.1 Regional Geology, Hydrogeology, and Structural Geology [40 CFR 146.82(a)(3)(vi)]

The BBE-P1 geologic sequestration site is located along the southeastern flank of the Gulf Coastal Plain, which is underlain by a thick succession of Cenozoic strata that recorded the evolution of drainage within the central part of North America (**Figure 1-1**). The coastal plain succession thickens and becomes younger into the Gulf of Mexico (GoM). A regional cross section of this area is provided as **Figure 2-1**. **Figure 2-2** shows the BBE-P1 site, including the existing infrastructure and wells, as well as the site bathymetry.

The GoM Basin formed during the Late Triassic and Early Jurassic Epochs as the North American tectonic plate rifted apart from the South American and African plates (Salvador, 1987). By Late Jurassic time, the Atlantic Ocean became linked with the GoM, resulting in widespread deposition of the Louann Salt (Salvador, 1987). During the early Cretaceous, the GoM experienced a low supply of clastic sediment, resulting in predominantly carbonate deposition (Winker and Buffler, 1988).

By Late Cretaceous through the Paleocene, a series of basins formed across the Western Interior Seaway, below what is now the Great Plains of North America, in response to Laramide Orogenesis (Galloway et al., 2000 and 2011). Laramide uplifts delivered abundant sediment into basins across Wyoming, Colorado, and New Mexico. At this time, limited mixed carbonate and siliciclastic deposition occurred in the northwestern GoM. After filling of the Laramide basins, an influx of sediment into the northern GoM Basin formed extensive fluvial and deltaic deposits that caused progradation of the continental margin into the GoM by tens of kilometers (Galloway et al., 2000 and 2011).

By latest Eocene time, deltaic sedimentation decreased until the Oligocene Epoch, when sediment-input volumes increased into what is now the present-day south Texas region (Galloway et al., 2000 and 2011), culminating in deposition of widespread Anahuac Formation near the end of the Oligocene. By early Miocene time, fluvial and deltaic deposition continued along the Gulf Coast region. Sediment supply into the GoM Basin was controlled by southeast-flowing river systems that eventually shifted to a dominantly southerly drainage pattern by Miocene time (Galloway, 2005).

Galloway defined a series of basin-margin "genetic stratigraphic sequences" that record distinct depositional episodes for the northwestern GoM Basin (**Figure 2-3**; Galloway et al., 2000 and 2011). Four basin-margin depositional episodes for the Miocene stratigraphic succession were based on regionally extensive marine flooding horizons (e.g., Olariu et al., 2019). Claimed as PBI

Claimed as PBI

Claimed as PBI

Principal depositional components of the lower Miocene include the development of the south-trending Newton fluvial system, which fed into the High Island or Calcasieu delta across the Texas–Louisiana border (**Figure 2-4**; Olariu et al., 2019; Galloway et al., 1986; and Galloway, 1989).

The large-scale depositional patterns that were established by the Miocene, continued into the Pliocene and Pleistocene. In the Plio-Pleistocene, deposition began to be strongly influenced by higher frequency and larger amplitude climatic variations that generated shorter genetic sequences which recorded an overall progradation of the Gulf Coast depositional system into the basin (Galloway et al., 2000 and 2011).


Claimed as PBI


Claimed as PBI

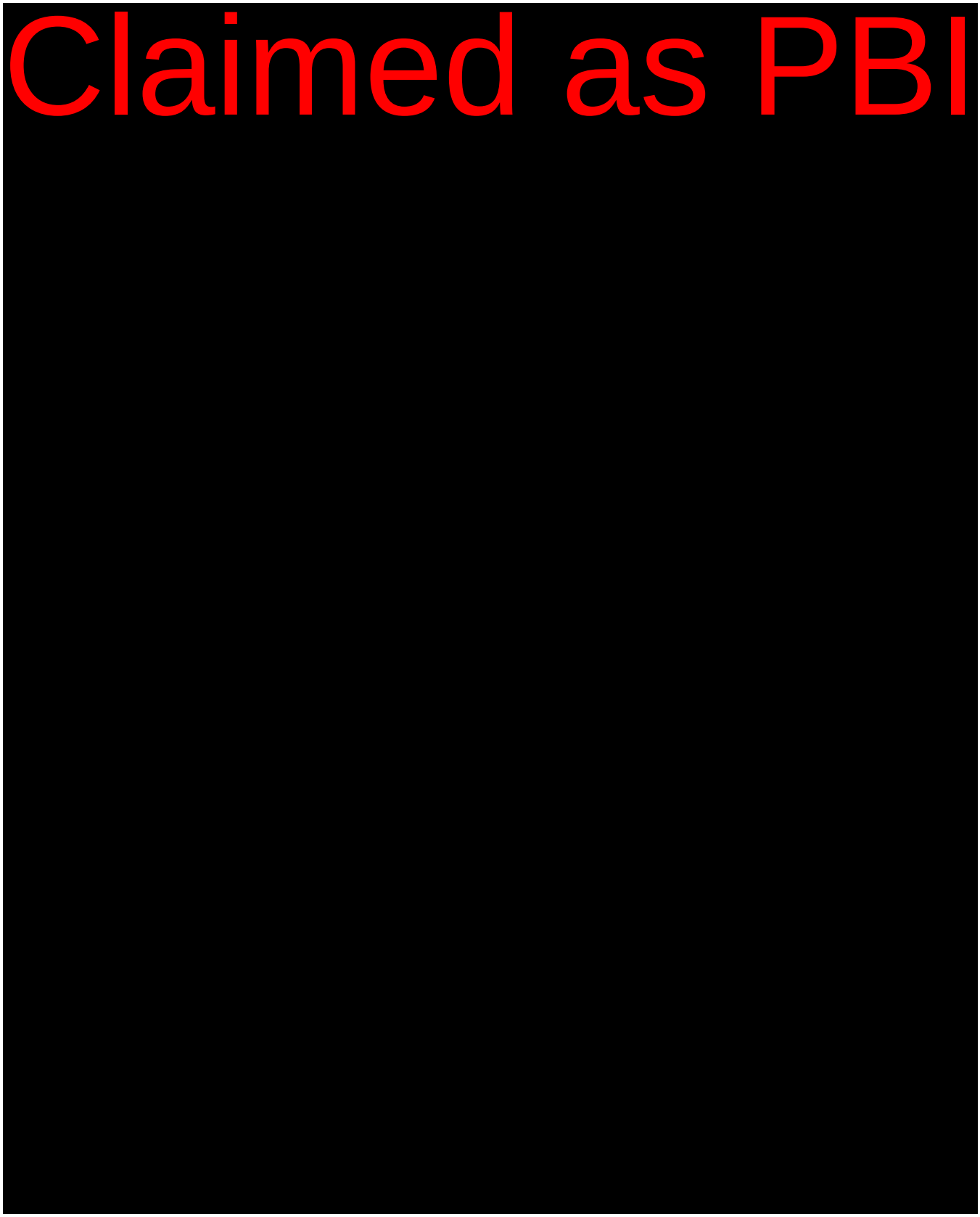
Claimed as PBI

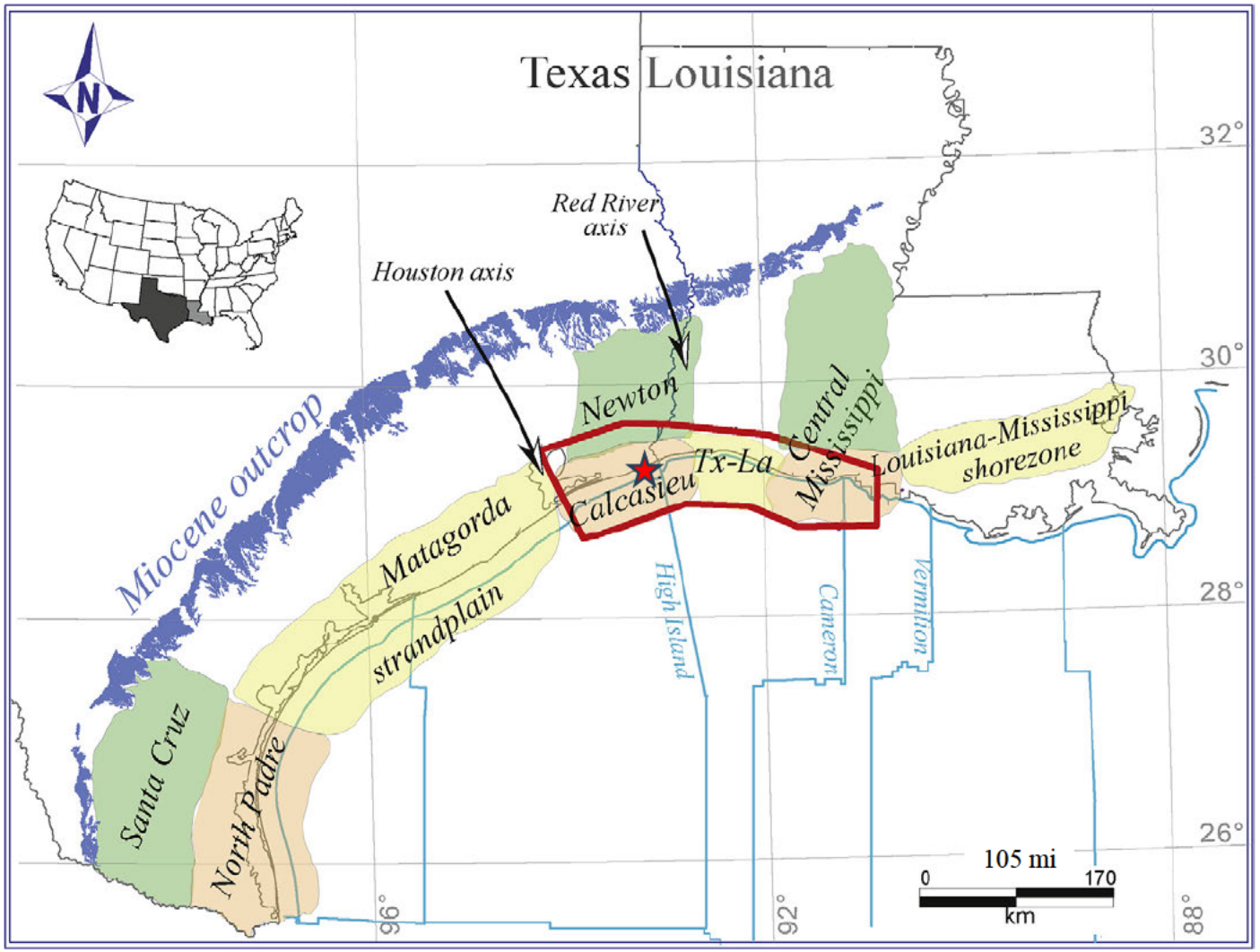

Figure 2-4: Location of updip Miocene outcrop belt and down-dip paleogeography of the Calcasieu Delta and Newton fluvial system (from Olariu et al., 2019). Red star denotes location of BBE-P1 site.

2.1.1 Stratigraphy

Gulf Coast deposits consist of sand, silt, and clay that record deposition in fluvial, shallow-marine, and deep-marine settings. The lower Miocene updip succession is dominated by fluvial deposition and these depositional successions become increasingly dominated by marine sedimentation downdip (**Figure 2-5** and **Figure 2-6**) (modified from Galloway et al., 1986). Compaction and variations in sediment supply and tectonic subsidence caused depocenters to shift the shoreline over time. Geological changes in depocenter activity resulted in lateral shifts in facies associations both along strike and dip. The overall geometry of the Texas coastal succession resulted in the preservation of thicker accumulations of sediment down dip, toward the GoM.

Miocene-aged lithostratigraphic units are exposed along the coastal plain as relatively broad, shore-parallel swaths (**Figure 2-4**) that dip toward the GoM. The geologic age of these regional surface geologic units are progressively younger towards the Gulf Coast. Generally, these morphostratigraphic belts define a coast-parallel depositional framework that has dominated much of the development for millions of years. In addition, the individual width of each depositional episode reflects its relative stratigraphic thickness in relation to other swaths and stratigraphic units (i.e., in general, the broader the outcrop swath, the greater the deposit thickness).

The stratigraphic succession described for the project area focuses on the Oligocene Frio Formation, Oligo-Miocene Anahuac (Shale) Formation, Miocene Fleming Group (Oakville and Lagarto Formations [Fms]) Miocene Goliad Fm, Mio-Pliocene Willis Fm, and the Plio-Pleistocene Lissie, and Beaumont formations (**Figure 2-3**). Thin Holocene alluvial and coastal marsh deposits are locally preserved (Baker, 1979; Young et al., 2012). These lithostratigraphic units have relatively consistent updip and downdip trends in depositional environment, overall lithology, and sand quality that serve as analogs for defining correlation frameworks and locating optimal injection sites **(Figure 2-1).**

The Oligocene Frio Formation represents a series of deltaic and marginal-marine deposits that are the down dip equivalent of the nonmarine Catahoula Formation. The Frio Formation is a major clastic wedge that prograded more than 60 miles into the GoM Basin. Progradation was followed by a period of aggradation and eventual retrogradation and end of the Frio depositional package marked by the Anahuac Formation (Galloway et al., 2000 and 2011). Shoreline conditions remained relatively constant during Frio deposition, resulting in the development of narrow and thick, homogenous belts of sand that comprise 25-40 percent of the cumulative Frio section, which locally exceeds 12,000 feet (ft) in thickness (Galloway, Henry, & Smith, 1982b).

Following Frio deposition, thick shale of the Oligo-Miocene Anahuac Formation was deposited during an extensive marine transgression across the Gulf Coastal Plain that occurred at the end of Oligocene. The resulting transgression left a thick succession of shale that acts as a regionally continuous stratigraphic seal. The Anahuac Formation is recognized 6,200 to 7,500 ft beneath the sea level in the project area and wedges out in the northern portion of the project area, beneath the present coastal plain (**Figure 2-5**) (Galloway, et al, 1986).

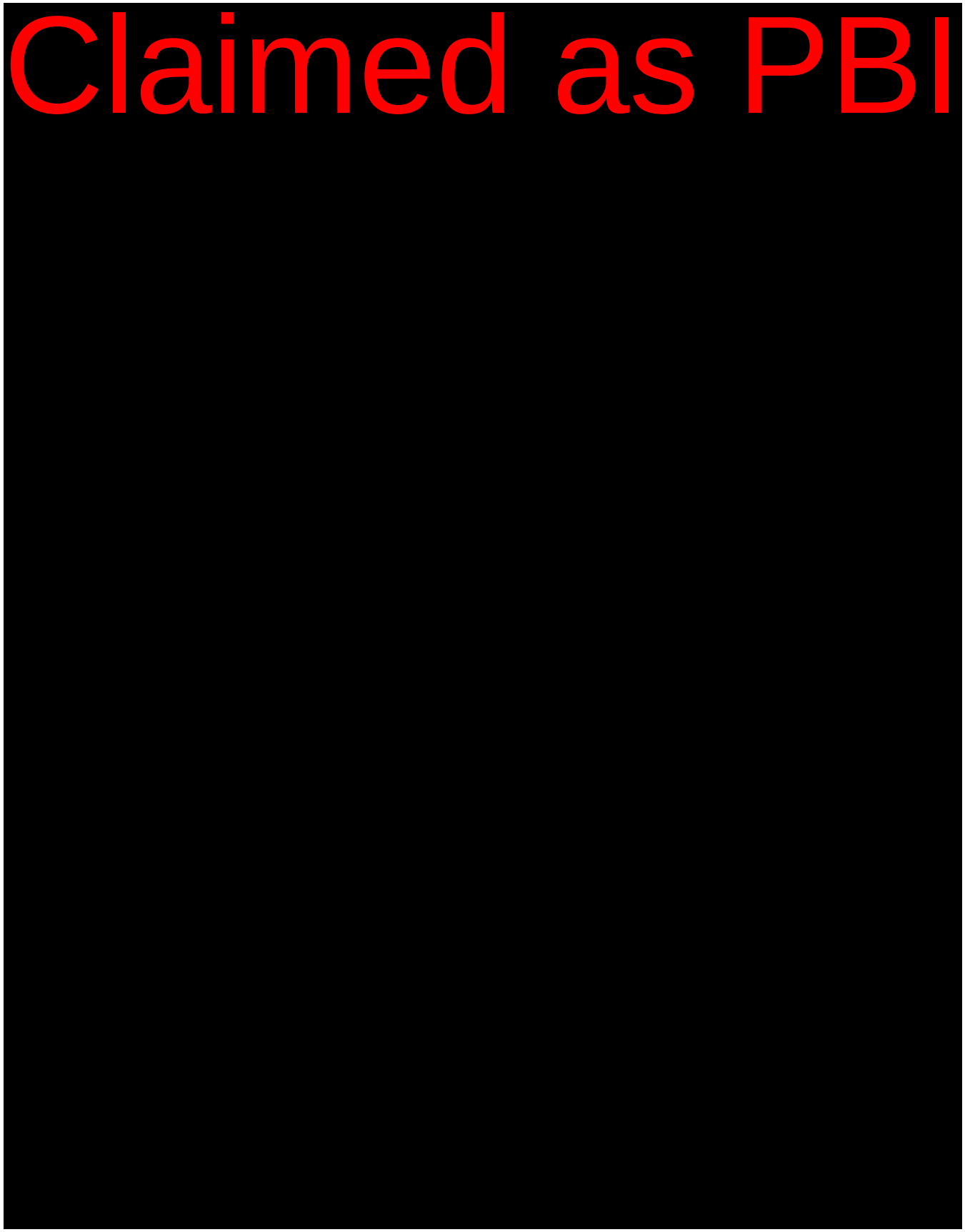
Claimed as PBI


Claimed as PBI

Overlying the Anahuac Formation is the Miocene Fleming Group, which contains the Oakville (LM1) and Lagarto (LM2) Formations **(Figure 2-3)**. Deposition of the Fleming Group occurred in shallow-marine environments across a broad, submerged, shelf-platform that developed during earlier Frio and Anahuac deposition. Three major depositional regimes characterize the Fleming Group: fluvial; deltaic; and marginal marine (Galloway et al. 1986).

Miocene formations along the Texas Gulf Coast are typically separated into Lower Miocene 1 (LM1), Lower Miocene 2 (LM2), Middle Miocene (MM) and Upper Miocene (UM) lithostratigraphic units. The Oakville Formation (LM1) and Lagarto Formation (LM2) exhibit a relatively consistent downdip (proximal-to-distal) progression of depositional environments and facies associations that are consistent with coastal plain and near-shore environments.

Deposits of the LM1 and LM2 are distinguished using benthic foraminifera associated with maximum flooding surfaces (MFS) that overlie major Miocene units (**Figure 2-3)**. The base of the LM1 unit is defined as the Anahuac Shale. The *Siph D* shale package within the Oakville Formation (LM1) is named after the foram *Siphonina davisi* and represents a regionally extensive flooding surface. The *Marg A* shale overlies the LM1 unit and is named after the foram *Marginulina ascensionensis*. The *Amph B* shale defines the shale overlying LM2 and represents a major marine transgression. Galloway et al. (1986) delineated 11 biostratigraphically defined flooding surfaces across the region that are labeled, in decreasing stratigraphic order: MFS1 through MFS12. Additional stratigraphic control comes from biostratigraphic subdivisions and mappable MFS across the Miocene succession (Olariu et al., 2019).

Lagarto Formation sandstone consists of fine- to very fine-grained sand composed mostly of quartz and less amounts of feldspar detritus (Curray, 1960). Shale contains clay minerals, including montmorillonite, kaolinite, illite, chlorite, and mixed-layer smectite-illite, whereas siltstone contains clay, silt, and very fine-grained sand (Curray, 1960).

Proximal (updip) rocks of the Oakville Formation are associated with terrestrial deposition and contain (calcium-carbonate) cemented sandstone and mudstone that were laid down in river channels, on floodplains, and as crevasse splays. Distal deposits represent deltaic, barrier island, lagoonal, strandplain, and marine shelf deposits composed of fine-to coarse-grained sandstone and interbedded shale. Seaward of the Oakville shelf edge, correlative sediments were deposited along the continental slope as upper-slope sandstone and shale that thicken on the downthrown sides of normal growth faults (Galloway, et al, 1986; Galloway, Henry, and Smith, 1982).

Proximal (updip) rocks of the Lagarto Formation are differentiated from the underlying Oakville strata by their overall finer grain size. Proximal regions of the LM2 (Lagarto Fm) generally contain muddy, stacked fluvial and coastal plain sediments. Downdip, LM2 deposits coarsen and reflect deposition in fluvial, deltaic, and barrier environments. As with the underlying LM1 (Oakville Fm), the Lagarto shelf and upper-slope fine-grained sandstone and mudstone thicken across normal growth faults into the GoM Basin **(Figure 2-1)** (Galloway et al., 1986). Deposits of the lower Oakville Formation are the result of offlap as the Fleming Group shoreline migrated basinward across the older Frio shelf. Younger strata of the Lagarto Formation are dominated by strong vertical stacking and minor backstepping due to later marine transgressions (Galloway et al., 1986).

The Miocene Goliad Formation is recognized regionally across the Texas Coastal Plain where it forms a basinward-thickening progradational wedge of fluvial and deltaic deposits that overlie the Fleming Group and older rocks (**Figure 2-3**). Galloway subdivided the Goliad Formation into his MM and UM genetic sequences (e.g., Galloway et al., 2000 and 2011). A shale containing *Textularia stapperi* (Text W) defines the top of the MM unit, the lower member of the Goliad Formation. The upper member of the Goliad Formation is defined by the *Rob E* shale. Regionally, the Goliad Formation ranges from 200 to >1,500 ft in thickness and consists of claystone, sandstone, conglomerate, and limestone.

The Mio-Pliocene Willis Formation unconformably overlies the Goliad Formation and older rocks. The Willis Formation is unconformably overlain by the Lissie Formation and locally by the Beaumont Group and undivided alluvial and coastal plain deposits. The Pleistocene Lissie Formation contains clay, silt, sand, and gravel laid down by meandering rivers. The Pleistocene Beaumont Group consists of multi-colored clays with limestone nodules and interbedded sand that ranges from 25 to 400 ft in thickness. The Beaumont Group unconformably overlies the Lissie Formation and underlies undifferentiated Holocene coastal marsh deposits along the Texas and Louisiana Gulf Coastal Plain **(Figure 2-3)**.

Below the Lower Miocene formations, the rapid accumulation of sediments into the basin fed by deltas led to the generation of over-pressured zones as rapid burial built up fluid pressures to a level where they exceeded hydrostatic pressures (Jones, 1969). The LM1 *Siph D* shale / Oligocene Anahuac Fm of over-pressured rock commonly forms the effective base of the CO_2 injection into the Cenozoic section and has been mapped across the Texas coastal zone by Pitman (2011).

Environment of Deposition (EoD)

Conceptual models provide a way to integrate well-log and seismic data into a three-dimensional framework that can be used to identify and model spatial relationships, reservoir architectures, connectivity, and heterogeneity trends. Paleogeographic reconstructions of the Gulf Coast Basin indicate fluvial- and wave-dominated deltaic sedimentation (e.g., Galloway et al., 2000 and 2001; Olariu et al., 2019) during deposition of Lagarto Fm (LM2). Examination of well log character with legacy well data and published paleogeographic reconstructions identified six distinct facies associations that are used to guide the construction of the static 3D model (**Table 2-1**). Seismic data has sufficient resolution to detect geomorphological features and the well log character is tied to seismic geomorphology to further validate EoD.

Facies associations are interpreted from well-log character within parasequence-sets defined by nine fine-scale horizons representing local flooding surfaces Claimed as PBI Predominance of well-log character and vertical transition of facies associations within the parasequence sets are used to define dominant environment of deposition per fine-scale zone (**Figure 2-7**).

Distributary channels are identified in well-logs as low gamma ray (GR) and low spontaneous potential (SP), sand-rich packages with sharp bases and sharp tops. Vertical trends within these packages are commonly blocky to upward fining. These deposits typically occurred directly overlying- or up-dip of mouth-bar and proximal delta-front facies associations.


Claimed as PBI


Claimed as PBI

Mouth-bars are identified as low GR and Low SP, sand-packages with upwards coarsening profile and sharp top. Well-log character is dominantly homogeneous, with minimal log serration. Sharp tops asso associated with these packages are commonly associated with overlying distributary channels and interpreted to reflect subsequent incision of the mouth-bar.

Proximal delta front deposits are identified as strongly upward-coarsening packages with upwards-decreasing serrated well log character. Bases are typically moderate-to-high sand content, expressed as moderate GR and SP values, but exhibiting clear serration. Well-log serration decreases upwards and becomes increasingly blocky and sand rich. This upwards decrease in serration is interpreted to reflect progradation of a delta-front deposit dominated by waning sediment gravity flows. These deposits are commonly directly overlying- or updip of distal delta front deposits.

Distal delta front deposits exhibit a strongly upward-coarsening, highly serrated well log character. Packages are typically sand-poor (moderate GR and SP) at the base and increase upwards to moderate sand content (moderate to low GR and SP). Well-serration is high and consistent from base to top, reflecting high vertical heterogeneity. These deposits are interpreted to reflect the distal component of prograding delta-fronts, where deposition is dominated by interbedded sandstones and siltstones resulting from waning sediment gravity flows.

Sand-prone delta/coastal plain and Incised Valley deposits exhibit thick, blocky, sand-rich packages of low GR and low SP with sharp bases and tops. Thicknesses of blocky packages are thicker than distributary channel packages and commonly occur in multiples that are amalgamated, locally separated by high GR, high SP shale-rich interbeds. Thicknesses and presence of shales varies across wells, suggesting irregular and non-correlative packages due to incision. Local thicknesses of these packages reach 200 ft, which is greater than proximal-delta front, mouth-bar, and distributary-channel deposits combined. These amalgamated packages with variable thickness and local occurrence of shales are interpreted to reflect deposition channelization within a sand-rich coastal plain. Incised valley fills are normally recognized in well logs and seismic by an abrupt thickening of sandstone on coarsening-upward mouth-bar and delta-front deposits. The thickness of these typically sharp-based paleovalley fills are generally greater than individual mouth-bars and delta-front successions that comprise shallow-marine parasequences.

Sand-poor delta/coastal plain deposits exhibit a well log character of interbedded blocky- to fining-upwards sand-rich packages separated by distinct shale-rich or interbedded/serrated packages. Sand-rich packages are commonly sharp-based and commonly show minimal internal serration at the base and more pronounced serration at the top. These deposits are interpreted to reflect a moderately shale-prone coastal/delta plain incised by delta-plain channels.

Seismic Character

Seismic resolution within the vicinity of the BBE-P1 project is high and was used to further validate environment of deposition interpretations from well-log character. Spectral decomposition and seismic amplitude were viewed in stratal slices and tied to well log character at parasequence set scale to detect geobodies to provide insights into depositional processes. Three dominated seismic geomorphological characters were identified (**Figure 2-8**) that align to the six facies associations in Table 2-1: Summary of interpreted Environments of Deposition (EoD) for the injection and confining zones**Table 2-1**:

- Deltaic lobe (distributary channel, mouth-bar, and delta-front deposits) (**Figure 2-8 C and D**)
- Incised valleys (**Figure 2-8 B**)
- Coastal plain channel deposits (**Figure 2-8 A**)

Spectral decomposition and red-green-blue color blending were used to increase detectability of geomorphic features by using both frequency and amplitude spectra within the seismic data. This was conducted due to the high-net yet interbedded character of the LM2 injection zone. Red-Green-Blue colors (**Figure 2-8 D-B**) correspond to unique, specified frequency ranges.

In spectral decomposition stratal slices, delta-lobe deposits **(Figure 2-8 D-C**) exhibit a distinct lobate geometry down-dip of a narrow channel-form feature. Commonly multiple of these deposits are laterally offsets within stratal slices, interpreted to be the result of compensational-stacked delta-lobes composed of distributary channels, mouth-bars, and delta-front deposits. Updip channel-form deposits are 0.1-0.5 miles wide and lobate mouth-bar and delta-front features are commonly 2-4 miles wide. Spectral decomposition character exhibits a radial change, indicating radial changes in stratigraphic heterogeneity, interpreted to reflect the progradational nature of these deposits.

Incised valleys are imaged as sharp-edged channel-form features 0.5-3 miles wide that continue the whole length of the area of interest (**Figure 2-8 B**). Lateral edges are sharp and distinct and vary from straight to sinuous. In cross section (**Figure 2-8 B-B'**), these deposits exhibit a scoured base that truncates reflectors and shows multiple internal scoured surfaces that are 160-250 ft thick. Collectively these observations indicate significant incision that was outsized relative to surrounding deposits and interpreted as incised valleys. The two incised valleys shown in **Figure 2-8** are included in the model.

Coastal plain channel deposits exhibit multiple laterally offset channel features 0.25-0.75 miles wide with high amplitudes (sand-rich) within a mottled, variable amplitude (heterogeneous to sand poor) background (**Figure 2-8 A**). Multiple channel-form features are identified on the stratal slices and show bifurcations, common regional but multiple local orientations, and are moderate to highly sinuous.

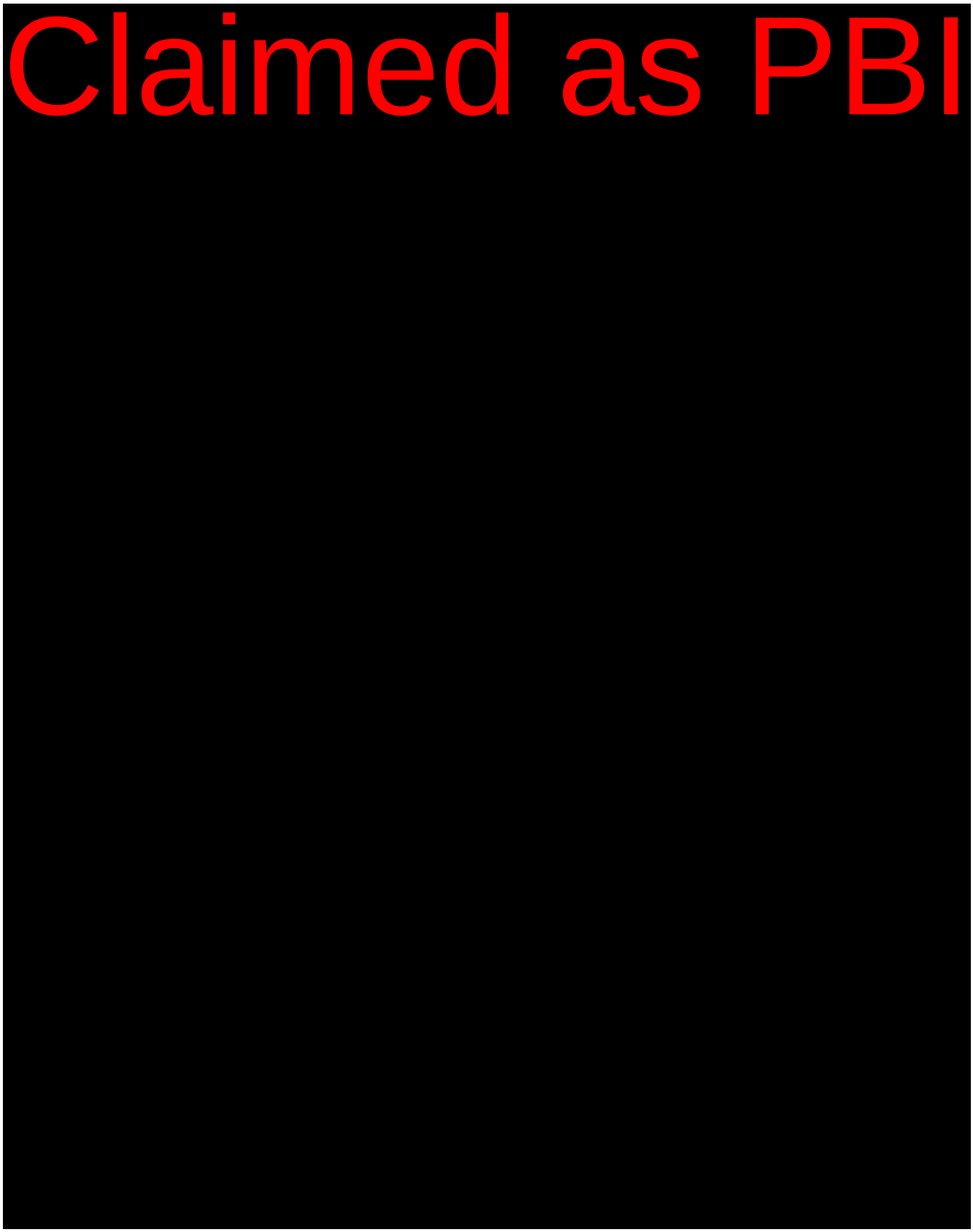
Claimed as PBI

2.1.2 Regional Structural Geology

Gravity has been the driving force in Gulf Coast tectonics since the opening of the GoM. When the GoM opened in the Jurassic Period, the Gulf Coast region became a trailing continental margin that foundered and subsided (Hall et al.,1982). Sediments accumulated on the margin and adjacent oceanic crust, which caused further subsidence in response to the sedimentary loading. Continual subsidence has created depocenters for additional sediment accumulation, which has produced the thick wedge of clastic sediments that continue to increase in thickness, as well as prograde further into the basin (Hall et al., 1982).

On a regional scale, growth faulting and diapirism of salt or shale (**Figure 2-9)** are the principal structural mechanisms of the Gulf Coast. Each is the result of sediment loading creating instability in the strata. The potential effects of each mechanism on the structural setting of the BBE-P1 site are discussed below. Structural cross sections in the strike and dip orientations, respectively **Figure 2-13** and **Figure 2-14,** will be referenced in the discussion that follows. Salt domes are common along parts of the Texas Gulf Coast (Ewing, 1991). These diapirs form as salt from the Jurassic Louann salt rise through overlying strata to form spires, banks, and domes that are responsible for local increases in water salinity.

Gravity-induced tectonism is relatively passive, characterized by the dominance of tensional forces and relatively low seismicity. Similarly, faulting of the type generally seen in the Gulf Coast tends to initiate in areas of high sedimentation rates, particularly along shorelines and along shelf margins. Once the center of deposition shifts to a new location (for example, when the position of a river mouth shifts laterally due to avulsion), the fault movement that has resulted from the buildup of sediments at the former location tends to diminish and eventually ceases. Faulting occurs when large masses of unconsolidated sediments at the outer shelf margin slump downward and laterally into adjacent basins (Van Siclen, 1967; Bruce, 1972; O'Neill & Van Siclen, 1984). This movement along faults results in the displacement of large volumes of sediments over distances that range from a few feet to several miles. Because these tectonic processes generally occur gradually over time, and the strata being affected are ductile to slightly brittle, the stresses released generate little or no seismogenic activity (Van Siclen, 1967; Bruce, 1972; O'Neill and Van Siclen, 1984).

Additional geologic structures are related to growth faulting, mainly in response to sediment loading where poorly consolidated sediment loads the underlying strata to a point of gravitational instability and collapse. Individual faults tend to be somewhat arcuate and have displacements ranging from hundreds to thousands of feet. Larger fault systems are composed of numerous interconnected faults that collectively may extend for tens of miles along strike (Weber, 1975; Kreitler, 1988).

Claimed as PBI

Claimed as PBI This higher ratio of shale is appreciably larger for the upper confining units, thus, enhancing the sealing aspect of these growth faults. The lithology and lateral continuity of the upper confining units, which include the containment interval and the confining zone Claimed as PBI is demonstrated on the structural cross sections described below (**Figure 2-13** and **Figure 2-14**).

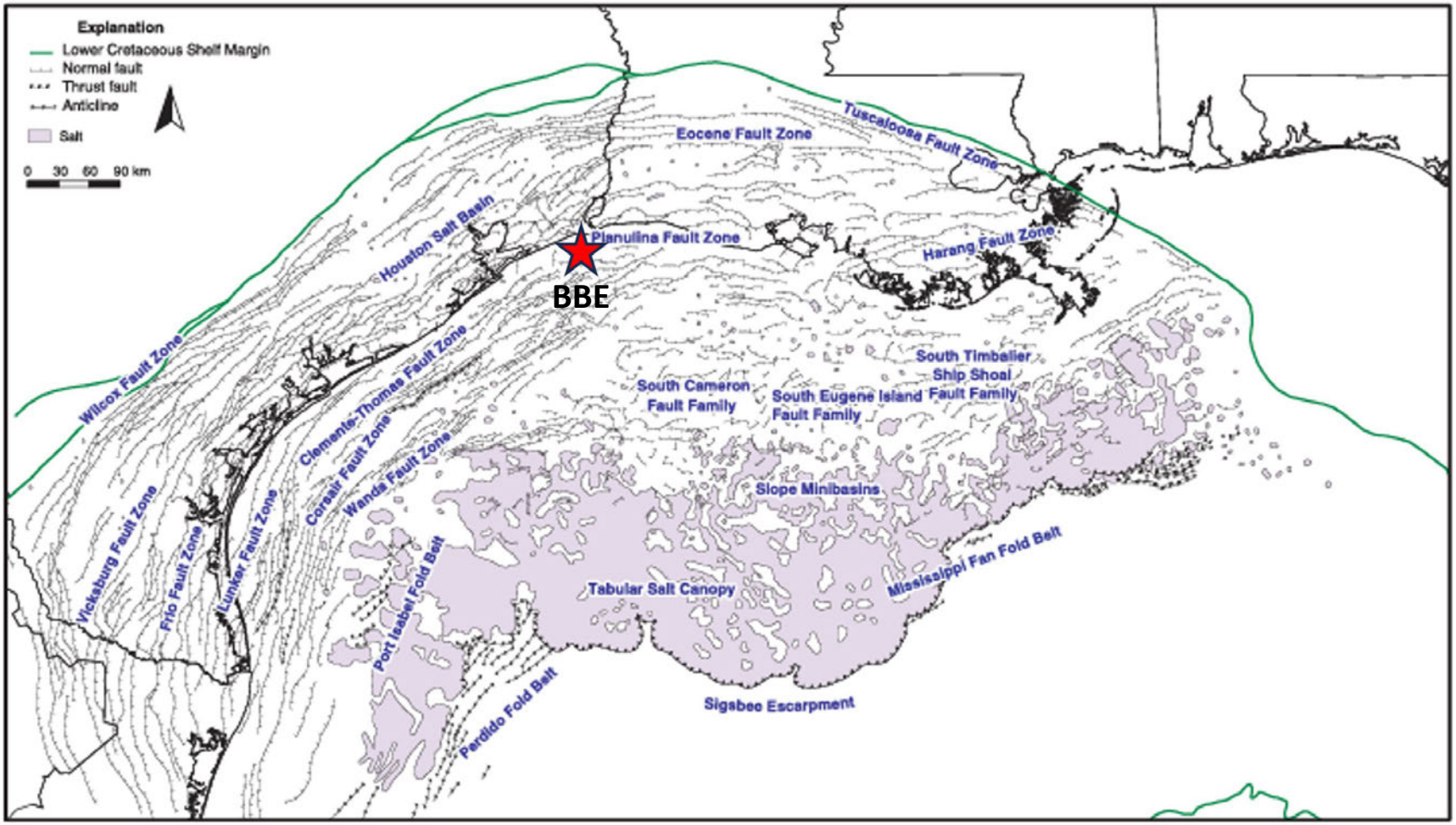

Figure 2-9: Structural context and extensional faulting at BBE (star) and surrounding areas. Modified after Galloway (2008) and Watkins et al. (1995).

2.1.3 Regional Faults and Fractures

Figure 2-10 provides a cross sectional view of the BBE project area. Claimed as PBI

Claimed as PBI

The prevalence of shale and the existence of shale-to-shale contact across faults above the proposed injection intervals are displayed in the cross section **Figure 2-10.**

In the confining zone, shale is juxtaposed against shale across the fault (**Figure 2-10**), with low-permeability fill. Clay smear is likely to occur in the fault plane, as discussed below. These conditions will aid in the prevention of vertical migration through the faults and confine wastes to the injection zone.

Clay smear occurs commonly in fault zones with layered sands and shales. Overburden pressure on beds undergoing normal faulting is greater than the pressure in the fault zone. If the shale is fluid enough and the fault moves slowly enough (Naruk, et al., 2002), plastic shales squeeze into the fault zone, resulting in clay smeared along the fault. Intervals with 40% clay can form clay smears. An outcrop study in New Mexico found that clay smears tend to be continuous for two to six times the thickness of the clay source bed (Cerveny, et al., 2005). Furthermore, "the thickness of the clay smear along the fault increases with the thickness of the source shale bed and decreases with distance from the source shale" (Cerveny, et al., 2005). Shale smear in a fault zone can therefore be almost continuous along the length of the fault in sequences of alternating sands and shales, except opposite thick sand beds. Shale smear may be discontinuous along the fault plane across thick sand beds as the distance from the smearing shale layers increases.

Additionally, shale smear will reduce porosity and permeability (Cerveny, et al., 2005). Whether clay is present in the fault zone or not, reduced permeability in the zone retards the vertical movement of fluid via faults.


Claimed as PBI

2.1.4 Regional Hydrogeology

The onshore Gulf Coast aquifer system of eastern Texas, a series of shoreline-parallel aquifers of variable salinity, is located updip from BBE-P1 (**Figure 2-11**; **Figure 2-12**). Claimed as PBI [redacted] **Figure 2-3**). Downdip equivalent formations offshore have similar geologic characteristics (Section 2.1.1; **Figure 2-3**); however, are observed at deeper depths and based on petrophysical calculations, higher salinity content (Section 2.7.1).

The Gulf Coast aquifer system consists of a broad low-relief coastal plain that gently rises from sea level to coastal uplands in the north, which are up to 900 ft above sea level (Chowdhury and Turco, 2006). The Gulf Coast aquifer system consists of a thick succession of homoclinally dipping stratigraphic units that are recharged by the major rivers of Texas, including the mouth of the nearby Sabine River (Young et al, 2012). There are five hydrostratigraphic units identified along the Gulf Coast of Texas, listed below from oldest to youngest: Catahoula Aquitard; Jasper Aquifer; Burkeville Aquitard; and the Evangeline and Chicot Aquifers (Baker, 1979; Williamson and Grubb, 2001; and Young et al., 2012). **Figure 2-11** shows a hydrostratigraphy column that includes Lower Miocene aquifers: Jasper Aquifer and Burkeville Aquitard.

The Catahoula Aquitard is comprised of the Oligoene Frio and Anahuac Formations, corresponding to the Catahoula Group observed at BBE. At BBE-P1, the Catahoula Aquitard contains sparse sandstone and generally acts as a barrier to flow between the overlying Jasper Aquifer and deeper aquifers.

The Jasper Aquifer contains porous and permeable sandstone units that are thick enough to constitute a regional water-bearing interval. Sandstone of the Oakville and Frio Formations mark the base of this aquifer, whereas the top of the Jasper Aquifer is alternately defined within the Oakville, at the top of the Oakville, or in the overlying Lagarto Formation. Due to this variation and the general updip thinning, aquifer thickness ranges from 200 ft to over 3000 ft. Water quality in the onshore formation varies from fresh (<1,000 milligram per liter [mg/L]), in updip areas near sources of recharge, to moderately and highly saline (>3,000 mg/L), in downdip areas away from recharge areas (Young et al., 2012). Claimed as PBI [redacted]

Overlying the Jasper Aquifer is the Burkeville Aquitard. The Burkeville Aquitard consists of siltstone and claystone separating the aquifers in the underlying Oakville Formation from those in the Lagarto Formation or overlying Goliad Formation. Depending on sandstone quality encountered in the Oakville and lower Lagarto, the base of the Burkeville Aquitard is variably defined within the Oakville or lower part of the Lagarto Formation. The top of the Burkeville Shale varies from within the upper Lagarto Formation upsection to the base of the Goliad Sandstone. Overall thickness of the Burkeville aquitard is commonly between 300 and 500 ft (Baker, 1979).

The Evangeline Aquifer overlies on the Burkeville Aquitard and includes the Goliad Formation. The base of the Evangeline Aquifer locally extends into the Lagarto Formation where thick, porous, and permeable water-bearing sandstones are recognized. Evangeline Aquifer thickness ranges from as little as 400 ft on the outcrop and in the shallow subsurface to approximately 200 ft in the deep subsurface near the modern

coastline. Water quality onshore varies from fresh (<1,000 mg/L) to slightly saline (1,000– 3,000 mg/L), with salinity increasing generally with depth and distance from recharge areas (Young et al., 2012). Claimed as PBI

The Chicot Aquifer overlies the Evangeline Aquifer and includes Mio-Plio-Pleistocene formations and unnamed lithologic units. The Chicot Aquifer is typically sandier than the Evangeline Aquifer and exhibits multiple static water levels. Thickness varies from zero where the Evangeline crops out to more than 1000 ft at the present coastline. Claimed as PBI Chowdhury et al., 2006; Young et al., 2012).

Coastal groundwater systems typically have an onshore tapering saline wedge that occurs below fresher terrestrial groundwater. Relatively narrow mixing zones of fresher and more saline groundwater occur along the boundary of the salt-water groundwater wedge (Cooper, 1964).

Claimed as PBI

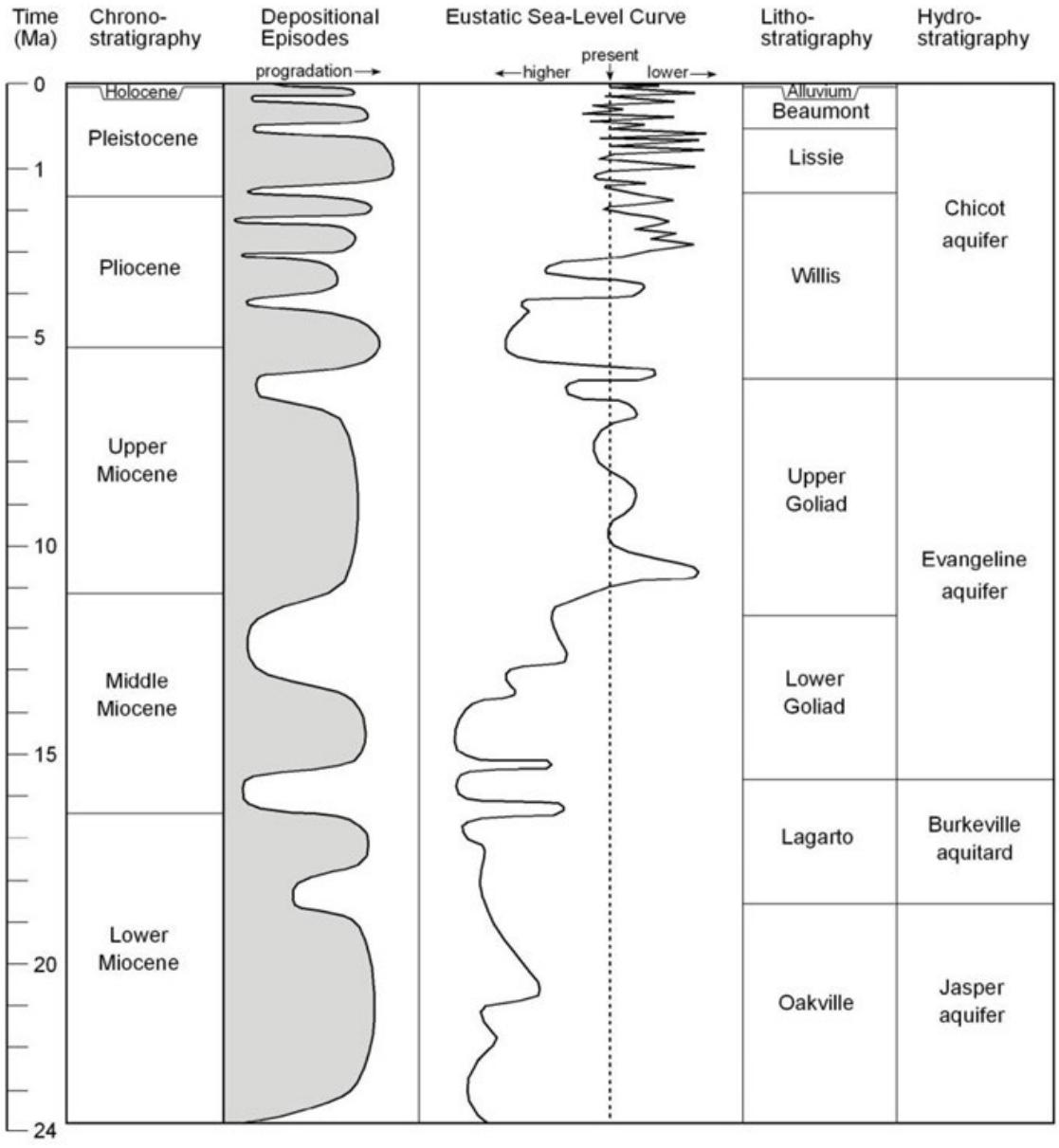

Figure 2-11: Chronostratigraphic chart of Miocene to Holocene depositional episodes, northwest GoM. Lithostratigraphic and hydrostratigraphic boundaries are approximate. Depositional episodes from Galloway et al. (2000) and sea-level curve from Haq et al. (1987). Geologic ages in millions of years ago (Ma) from Berggren et al. (1995). **(**From Young et al., 2012**)**

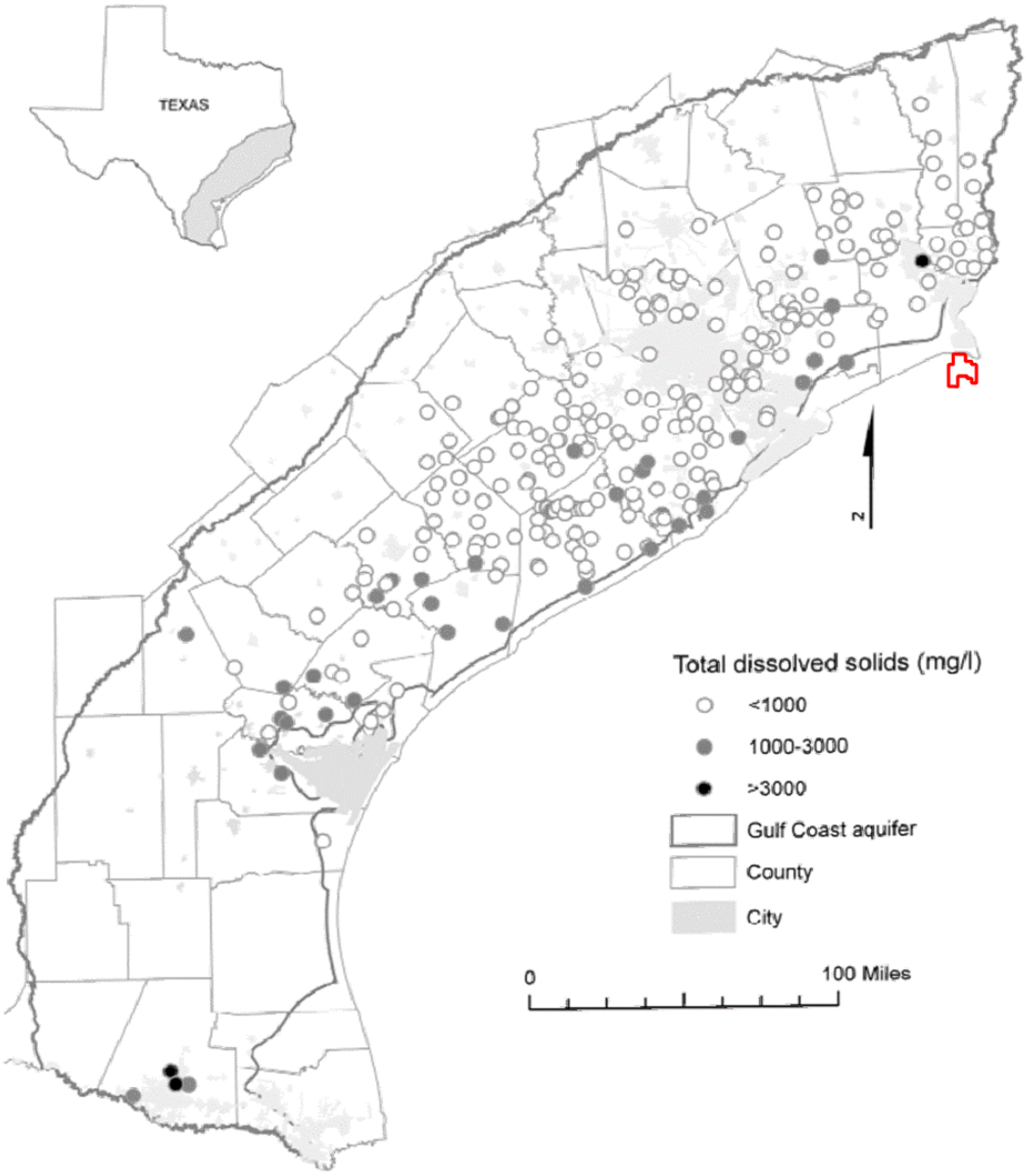

Figure 2-12: Distribution of total dissolved solids concentrations in the Chicot Aquifer. (from Chowdhury et al., 2006). BBE shown in red.

2.2 Maps and Cross Sections of the AOR [40 CFR 146.82(a)(2), 146.82(a)(3)(i)]

This section provides maps and cross sections per 40 CFR 146.82(a)(2) and (3)(i).

2.2.1 Local Cross Sections

Two structural cross sections are presented as **Figure 2-13** and **Figure 2-14**, representing sections in the dip and strike orientations, respectively. These cross sections illustrate the nature of the reservoir continuity and regional thickness of both the upper confining zone and the injection zone.

2.2.2 Local Structure and Isochore Maps of the Injection and Confining Zones

Local structure and isopach maps Claimed as PBI are provided as **Figure 2-15** and **Figure 2-16**, respectively. The structure map of the upper confining zone shows a low-angle dip from northwest down towards the southeast at approximately 1-3 degrees within the lease. Claimed as PBI [redacted] In general, the structure map of the injection zone shows a low-angle dip towards the southeast at Claimed as PBI [redacted]

The local structure map of the basal confining zone is provided as **Figure 2-19**. Claimed as PBI Claimed as PBI [redacted]


Claimed as PBI


Claimed as PBI


Claimed as PBI


Claimed as PBI


Claimed as PBI


Claimed as PBI


Claimed as PBI

2.3 Faults and Fractures [40 CFR 146.82(a)(3)(ii)]

BBE and surrounding area is an extensional regime of mixed Upper Eocene mud-prone and allochthonous salt detachments (Rowan, 1995; Galloway, 2008). Deformation in the area is similar in style and mechanism to the regionally-extensive Clemente-Thomas growth fault zone (**Figure 2-10**), which is an extensional growth fault system with maximum displacement, as much as 4000 ft (Treviño and Meckel, 2017), Claimed as PBI Hanging wall accommodation space is filled with synkinematic growth deposition, which can have a three-fold increase in cross-fault interval thickness.

At BBE-P1, these features are observed to a lesser magnitude, with maximum displacement and growth deposition observed in the Oligocene Frio along listric growth faults. These fault systems are commonly associated with minor splays and antithetic faulting (**Figure 2-20**) typical of those observed regionally (Galloway, 2008).

2.3.1 Fault Characterization and Style

Claimed as PBI . Faults were categorized and prioritized based on a set of interpretation criteria:

1. Radial extensional faulting with associated diapirism
    - Salt diapirs and related withdrawal synclines are common in the Gulf Coast Basin Claimed as PBI Claimed as PBI A local minibasin and associated extensional faulting occurs in a radial pattern surrounding this feature. Some of the associated faults extend into the BBE acreage (**Figure 2-20**, inset B). These faults tend to exhibit higher than average displacement (**Figure 2-21**) and may extend up to the shallow limit of seismic resolution.
2. Locally extensive growth faults
    - These faults originate from regional mud-prone Eocene detachment surfaces and are through-going into the overburden intervals (**Figure 2-20**, insets B and C). Maximum growth and displacement are accommodated by Paleogene sediments. While there are regional changes in Miocene thickness, cross-fault thicknesses are typically constant, indicating post-kinematic faulting local to the project area.
3. Synthetic normal faults
    - In addition to the deeply detaching growth faults, synthetic extensional faults are common. These faults may detach at variable levels within the mud-prone Paleogene intervals Claimed as PBI Claimed as PBI
4. Antithetic normal faults
    - Local antithetic normal faulting is commonly associated with salt withdraw and minibasin Claimed as PBI Claimed as PBI


Claimed as PBI


Claimed as PBI

2.3.2 Fault Displacement

Fault property analysis was performed in Petrel© 2022 using volume-based structural modeling. Horizons are interpreted to fault intersections, where they are offset and continued on the opposite side of the fault. Slip displacement, sometimes referred to as simply displacement herein, is defined as the total translational offset of a horizon or interval across a fault plane. This is not to be confused with fault throw, which is defined as the vertical displacement from the fault-plane intersection of a stratigraphic horizon on the footwall to the same respective horizon intersecting the fault-plane on the hanging wall.

2.3.5 Fault Clay Content and Seal Potential

Based on proven accumulations of conventional oil and gas deposits (Galloway et al., 1986), the extensional fault systems of the Lower Miocene are presumed to have excellent seal potential for carbon storage reservoirs (Silva et al., 2023). High fault clay content of interbedded shales and mudstones contribute to fault seal potential in the BBE acreage. In the containment interval and the confining zone, the combination of fault displacement and zone thickness occasionally results in shale on shale juxtapositions and reservoir (flow unit) juxtapositions against low-permeability basin fill. Fault juxtaposition of shale also indicates the likelihood of clay smear along the fault plane (e.g., Vrolijk et al., 2016), which may act as a fluid barrier to

lateral and vertical flow. These conditions likely prevent vertical migration up the faults and confine CO_2 to the injection zone.

Claimed as PBI

2.3.6 Fault Clay Content, Shale Smear, and Gouge

Fault zone clay content is the proportion of clay admixed within the fault zone, contributing to fault capillary seal potential. This property, also referred to as shale gouge ratio (SGR), is calculated from the volume of clay in deformed host rock intervals, thickness, and magnitude of slip (offset) of the respective intervals (Yielding et al., 1997). The SGR property can be computed within a structural model, when clay volume (Vclay) is calculated as a proportion of shale volume (Vshale). The higher abundance of shale in the stratigraphy, the higher the proportion of Vclay and thus, SGR, contributing to fault seal potential.

Recently published simulation results (Silva et al., 2023) offer analogs for BBE-P1. Claimed as PBI Claimed as PBI Their results show a range in SGR values from 58% to 82% and multiple injection scenarios, where small amounts of CO_2 have the potential for cross-fault lateral migration over the project lifespan (modeled in one scenario). The authors note that there are no scenarios where vertical fault migration is observed. Claimed as PBI Claimed as PBI

Claimed as PBI

2.3.7 Fault Transmissibility

The influence of faults on fluid flow presents a challenge in reservoir simulation. The combination of displaced lithologies across the fault plane and the properties of the fault rock and fault zone are difficult to constrain and scale to a reservoir model. Common practice in reservoir simulation is to apply a transmissibility multiplier (TM) (Manzocchi et al., 1999) to calculate fault transmissibility at a cellular level. This method scales physical properties of the fault and host rock to the model by incorporating the grid size as a distance metric. Typically ranging from 0 to 1, the TM is a scalar adjustment due to the material within the fault zone.

A range in grid and fault permeabilities was used to model transmissibility multipliers for the BBE-P1 model and to capture uncertainty in the physical constraints on fault transmissibility (host rock permeability, fault rock permeability, and fault thickness). Inputs to the transmissibility multipliers include SGR (discussed above) fault thickness, and fault permeability.

2.3.8 Fault Permeability

In the absence of direct fault rock permeability measurements, globally published expressions relating SGR to fault rock permeability (Manzocchi et al., 1999, Sperrevik et al., 2002) were used to constrain a range for modeling BBE-P1 fault properties. The average modeled fault permeability in the region of the BBE site acreage varies by two orders of magnitude between the two models. This is expected based on the ranges and maximum permeabilities represented by the two global models.

The Sperrevik et al. (2002) model requires the maximum burial depth of the modeled intervals and the depth at time of deformation, both in meters. Aligned with the approach documented in Silva et al. (2023), shallow burial depth (200 meters) was used to represent the timing of deformation. The present-day overburden is presumed to represent maximum burial depth.

2.3.9 Fault Thickness

Fault thicknesses can be inferred based on a positive covariation with displacement. A ratio of 1:100, fault thickness to displacement, is a standard default and was used to calculate spatially varying fault transmissibility multipliers in Petrel© 2022. This ratio aligns with globally observed thickness to displacement ratios for fault rock (e.g., Childs et al., 2009).

2.3.10 Fault Transmissibility Multipliers for Simulation

Using the input parameters described above, spatially varying TM results were generated in Petrel© 2022.

To capture uncertainty, TMs were calculated using twelve permutations: average values for grid permeability (high, medium, low), fault permeability (high, low) and fault thickness ratios (1:100 and 1:10). The results show a wide range in values with just over two orders of magnitude, in accordance with the broad range of inputs. The range is driven by the lithologic heterogeneity of cross-fault stratigraphy and the variable displacement accommodated by each fault.

Claimed as PBI

2.3.11 Fault Stability

A subset of 17 faults located in or next to the lease area was selected to perform a stability analysis (**Figure 2-22**). For this analysis, the stresses computed from the numerical Mechanical Earth Model (MEM) were projected into the fault surfaces and used to compute both the effective normal and tangential or shear

stresses acting on the faults. Because the faults are not perfect planes but have some waviness, the fault surfaces have been discretized into triangular elements of about 30 m size, and the stress projection has been done in each of the individual triangles using the MEM stresses from that location.

Results of the analysis are shown in **Figure 2-23**, **Figure 2-24** and **Figure 2-25** (the faults have been separated in three groups for clarity), in the form of shear vs effective normal stress diagrams in the so-called Mohr space. Each point represents the state of stress in one of the triangular elements. The points are color coded according if they belong to the Claimed as PBI or other formations located above or below (blue).


Claimed as PBI


Claimed as PBI


Claimed as PBI


Claimed as PBI

2.4 Injection and Confining Zone Details [40 CFR 146.82(a)(3)(iii)]

This section describes the overall geologic character of the injection and confining zones to support storage.

Claimed as PBI

Claimed as PBI


Claimed as PBI


Claimed as PBI

2.4.1 Proposed Upper Confining Zone

The primary upper confining zone Claimed as PBI

Claimed as PBI

2.4.2 Proposed Injection Zone

The proposed injection zone Claimed as PBI

Claimed as PBI

Claimed as PBI

2.4.3 Proposed Injection Intervals

Claimed as PBI


Claimed as PBI


Claimed as PBI


Claimed as PBI


Claimed as PBI

Claimed as PBI

2.4.4 Proposed Lower Confining Zone

The lower confining zone Claimed as PBI

Claimed as PBI


Claimed as PBI

2.5 Geomechanical and Petrophysical Information [40 CFR 146.82(A)(3)(IV)]

Predictions of the stress magnitudes and orientations as well as the fracture gradient were calculated using a finite-element MEM. The MEM covered an area of approximately 50x50 kilometer around the lease area and includes identified formations from the ground surface (or seabed) until 22,000 ft true vertical depth below sea level (TVDSS).

Claimed as PBI

Claimed as PBI

Claimed as PBI An overpressure ramp starting at the base of the T5 sand has been inferred from leak-off tests (LOT) data (**Table 2-4**) collected from various wells in the High Island area (**Figure 2-32**), as well as from offset well logs. Claimed as PBI

Claimed as PBI

Table 2-4: Available LOT data from offset wells.

Well	UWI	MD (ft)	TVDSS (ft)	LOT Grad (pounds per gallon [ppg])	LOT Press (psi)
HI 19 OCS G22227 001 ST00BP00	427084061200	4000	3909	14.1	2930
HI 22 OCS G05006 A001 ST00BP00	427084064300	4553	4429	14.8	3405
HI 22 OCS G32744 A001 ST00BP01	427084064301	10550	9711	17.0	8685
HI 37 OCS G20656 A004 ST00BP00	427084056700	10250	10158	17.1	9104
HI 37 OCS G20656 A004 ST00BP00	427084056700	13994	13901	18.5	13447
HI 52 OCS 00508 C003 ST00BP00	427084061400	9325	9060	17.3	8260

Claimed as PBI

Natural fractures have not been identified in the area of study, due to lack of wellbore images. Given the ductility of the formations, it is expected that natural fractures will not be very prevalent in the area of study. Large geological faults have been identified from the seismic data and they are extensively discussed in Section 2.3.


Claimed as PBI

2.5.1 Karst

No carbonates have been observed in the area of study, so the presence of karsts is not relevant for this project.

2.5.2 Local Crustal Stress Conditions

The stress regime for the BBE-P1 site was identified to be normal or extensional, with the main tectonic drive being the extension towards the GoM (Lundstern and Zoback, 2016). A second tectonic component is provided by the salt bodies, although these are localized effects expected only around and above the different diapirs found in the area, as evidenced by the orientations of the several faults identified within the area of study (**Figure 2-15**).

Claimed as PBI

Claimed as PBI This low anisotropy is expected in this tectonic environment and considering the low strength of these rocks.

2.5.3 Determination of Vertical Stress (Sv) from Density Measurements

Claimed as PBI


Claimed as PBI

2.5.4 Maximum and Minimum Horizontal Stress Azimuth

Under the assumption of an extensional stress regime, it is expected that the predominant maximum horizontal stress azimuth will be approximately parallel to the shoreline (i.e., E-W to NE-SW), and the predominant minimum horizonal stress azimuth will be approximately perpendicular to it (i.e., N-S to SE-NW). Local stress rotations are expected near the salt diapirs present in the area.

2.5.5 Elastic Moduli

Claimed as PBI

Claimed as PBI

2.5.6 Injection Zone Fracture Pressure

Claimed as PBI

Calculating the value of this $\Delta\sigma$ is difficult as there is no valid theoretical relationship for it. Usually, the FPP is measured in-situ using a step-rate test (SRT) seen in **Figure 2-34**. And $\Delta\sigma$ is then calculated by knowing the value of S_{hmin}. Claimed as PBI

Claimed as PBI

2.5.7 Confining Zone Fracture Pressure

According to the numerical models, the mean value of minimum horizontal stress gradient in the confining zone Claimed as PBI

Claimed as PBI

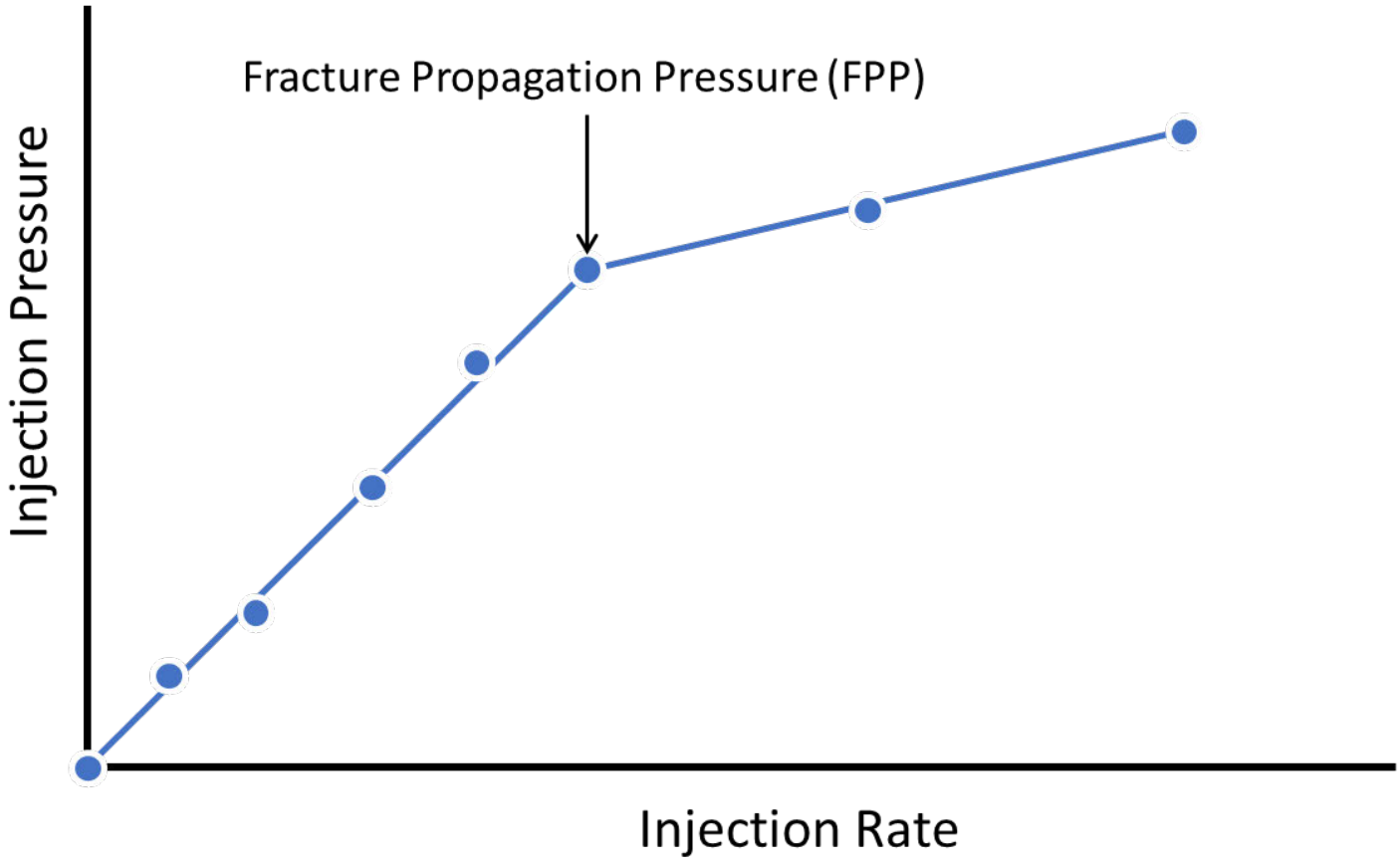

Figure 2-34: Typical pressure vs rate curve for a step-rate test (SRT). The injection rate is increased in discrete steps and at each step, the bottomhole pressure is recorded after it stabilizes. The injection rates and corresponding stabilized pressures are plotted, and they usually align with a straight line. A change of slope is usually observed at certain pressure, which corresponds to the pressure at which a fracture created at the wellbore starts propagating. This is known as the fracture propagation pressure (FPP). Once the fracture begins propagating, the subsequent points in the pressure vs rate plot align with a different straight line with a shallower slope.

2.6 Seismic History [40 CFR 146.82(a)(3)(v)]

A review of historical seismicity in southeast Texas was completed using the online monitoring databases of the United States Geological Survey (USGS) Earthquake Hazards Program and the University of Texas BEG's TexNet Earthquake Catalog (USGS, 2023 and TexNet, 2023). Data was filtered from the earliest events recorded to July 27, 2023, and encompassing a 100 mile radius around BBE. Available data (events and seismic stations) are presented in **Figure 2-35**, including the details of the nearest seismic event.

No events have been recorded within a 50-mile radius of BBE, and only one event was located within a 100-mile radius. This single Magnitude 3.8 event occurred in 1983 near Sulphur, Louisiana, at a reported depth of 8.7-miles (Stevenson and Agnew, 1988). It was recorded on the local Sweet Lake network approximately 5-miles to the southeast, an array sponsored by the U.S. Department of Energy for geothermal test sites. The event is believed to have occurred near the basement along the east-west trending Lake Arthur fault system which has a southeast dip. No substantiated damage was reported, and most public observations included minor rattling or movement of objects.

Based on recent North American stress modeling (Snee, 2020) and the available earthquake catalogs, the Gulf Coast region is characterized by low-frequency, low-magnitude seismic activity related to its extensional setting. The Gulf Coast geosyncline is comprised of "southerly dipping and thickening [Tertiary-age] beds disrupted by diapiric structures and regional systems of relatively shallow listric growth faults roughly paralleling the coast" (Stevenson and Agnew, 1988). Maximum horizontal stress (S_{Hmax}) direction follows the east-west trend of these growth faults (Snee 2020), dominated by north-south extension. While some present-day movement may occur along the faults, the poorly consolidated Tertiary sediments tend to deform plastically, and stress build-up is dissipated via continuous slippage or creep (Qu et al. 2019). Therefore, there is little potential for stress build-up along Gulf Coast faults and the risk of induced seismic is minimal for BBE-P1. This conclusion is further supported by the USGS's National Seismic Hazard Map (**Figure 2-35**) in which risk is very low (<4) along the Texas coastal plain.


Claimed as PBI

2.7 Hydrologic and Hydrogeologic Information [40 CFR 146.82(a)(3)(vi), 146.82(a)(5)]

2.7.1 Regional Hydrogeology

The Gulf Coast aquifer system, located updip from BBE, has a groundwater flow towards the southeast and is divided into five hydrostratigraphic units: Catahoula Aquitard; Jasper Aquifer; Burkeville Aquitard; and the Evangeline and Chicot Aquifers (Baker, 1979; Williamson and Grubb, 2001; and Young et al., 2012). **Figure 2-11** provides a hydrostratigaphic column that includes the Lower Miocene aquifers: Jasper Aquifer and Burkeville Aquitard respectively within the Oakville and Lagarto Formations. Salt domes may locally increase groundwater salinity and overall TDS.

An underground source of drinking water (USDW) as defined in 40 CFR §146.3 is

> *...an aquifer or its portion: (i) Which supplies any public water system; or (ii) Which contains a sufficient quantity of ground water to supply a public water system; and (A) Currently supplies drinking water for human consumption; or (B) Contains fewer than 10,000 milligrams of total dissolved solids per liter...*


Claimed as PBI


Claimed as PBI

Groundwater Flow

The Gulf Coast Aquifer dominant groundwater flow is toward the southeast direction. Faults may act as lateral barriers or vertical conduits for groundwater flow. Additionally, salt domes may also have localized effects on groundwater flow. (Baker, 1979, Young et al., 2012).


Claimed as PBI


Claimed as PBI


Claimed as PBI

2.8 Geochemistry [40 CFR 146.82(a)(6)]

The mineralogical characteristics of the proposed confining and injection zones do not indicate a potential for deleterious, geochemical reactions (Zhang et al., 2019).

Claimed as PBI

2.8.1 Other Information (Including Surface Air and/or Soil Gas Data, if Applicable)

BBE is located within a dynamic coastal environment of Texas State Waters. These waters experience freshwater inputs from rivers, runoff from upstream agricultural and farming lands, longshore currents, natural hydrocarbon seeps, algal blooms, existing pollution slicks, fishing activities, and shipping activities which result in continual variations in seawater chemistry, salinity, temperature, and sediment load. The project is immediately southwest of the Sabine Pass Ship Channel, a medium-sized port with LNG tankers comprising nearly a third of calling vessels (MarineTraffic.com, 2024).

Claimed as PBI

2.9 Site Suitability [40 CFR 146.83]

The summary below is a description of how the proposed injection site meets the suitability requirements set forth at 40 CFR 146.83. Claimed as PBI

Claimed as PBI

Claimed as PBI

Construction materials for this project were selected based on the corrosive nature of the injectate. Corrosion monitoring of the injection wells will be conducted throughout the life of the BBE-P1 program. In addition, the mineralogical characteristics of the proposed confining and injection zones do not indicate a potential for deleterious, geochemical reactions. Compatibility testing of the injectate with the injection zone will be conducted following installation of the injection well(s).

3 AOR AND CORRECTIVE ACTION

An Area of Review (AOR) and Corrective Action Plan was prepared per the requirements in 40 CFR 146.82(a)(13) and 146.84(b). INTERSECT© was used for CO_2 sequestration simulation to understand CO_2 saturation and pressure front migration through time, delineate the AOR, and optimize development scenarios. A tabulation of wells within the delineated AOR that penetrate the confining zone was created and files were reviewed to determine if corrective actions are necessary [40 CFR 146.82(a)(4)]. A summary of computational modeling details is provided [40 CFR 146.84(c).

The AOR and Corrective Action Plan with associated tables, figures, appendices including well records and modeling details have been uploaded to the GSDT in support of this application.

AoR and Corrective Action GSDT Submissions

GSDT Module: AoR and Corrective Action
Tab(s): All applicable tabs

Please use the checkbox(es) to verify the following information was submitted to the GSDT:

☒ Tabulation of all wells within AoR that penetrate confining zone ***[40 CFR 146.82(a)(4)]***

☒ AoR and Corrective Action Plan ***[40 CFR 146.82(a)(13) and 146.84(b)]***

☒ Computational modeling details ***[40 CFR 146.84(c)]***

3.1 Modeling

The AOR and Corrective Action Plan outlines the data, processes, software, and simulation results used to delineate the AOR. The AOR and Corrective Action Plan details data sourcing and analysis that was leveraged to generate a representative model that has been used to forecast pressure response and CO_2 migration through the life of the project. The document also provides a report on the wide variety of sensitivities that have been analyzed and their corresponding impacts to the AOR.


Claimed as PBI

3.2 AOR and Corrective Action

3.2.1 Artificial Penetration Tabulation and Well Records

Claimed as PBI

3.2.2 Condition of Artificial Penetrations Within the AOR

Claimed as PBI

Water Wells Within the AOR

A water well record search was conducted through the Texas Water Development Board to identify potential well penetrations through the confinement zone. The search concluded no water wells are present within the AOR. Surface bodies of water and other pertinent surface features are included in accordance with 40 CFR 146.82(a)(2) on **Figure 3-2** and **Figure 2-2**.

3.2.3 Corrective Action Plan

Claimed as PBI


Claimed as PBI

4 FINANCIAL RESPONSIBILITY

The Operator is providing financial responsibility for performing corrective action, injection well plugging, PISC, site closure, and emergency and remedial response, per 40 CFR 146.85. The costs associated with each of the above activities are outlined and submitted, per 40 CFR 146.85(a)(2) in the Class VI UIC Financial Responsibility Demonstration. The financial endorsement documentation is also provided in the Class VI UIC Financial Responsibility Demonstration.

The Financial Responsibility Plan has been uploaded to the GSDT in support of this application.

Financial Responsibility GSDT Submissions
GSDT Module: Financial Responsibility Demonstration ***Tab(s):*** Cost Estimate tab and all applicable financial instrument tabs Please use the checkbox(es) to verify the following information was submitted to the GSDT: ☒ Demonstration of financial responsibility ***[40 CFR 146.82(a)(14) and 146.85]***

5 INJECTION WELL CONSTRUCTION

Claimed as PBI These wells have been engineered with appropriate materials to meet the structural integrity requirements of 40 CFR 146.86, to meet the Operator's internal standards for well design, and to minimize corrosion throughout the life of the project.

The full well construction details for the CO_2 injectors can be found in the Well Construction documents.

5.1 Proposed Stimulation Program [40 CFR 146.82(a)(9)]

Stimulation to enhance injectivity is not planned currently at BBE-P1 during initial construction. Data collected during the installation of the injection and monitoring wells will provide additional data for fracture gradient, pore pressure and injectivity to further inform analysis for stimulation needs.

Periodically, enhancement techniques may be necessary to maintain injectivity performance. The techniques may mitigate scale, precipitates, plugging or other impairment sources. Prior to any stimulation, the enhancement fluids will be laboratory tested to ensure compatibilities with reservoir fluids, injection fluids, and tubing and casing materials. These enhancements will remain below 90% of fracture gradient threshold.

If stimulation is needed in the future, a plan will be developed and submitted for review and approval by the UIC Program Director prior to conducting any stimulation.

5.2 Construction Procedures [40 CFR 146.82(a)(12)]

5.2.1 Operating Data

Source of CO_2

CO_2 for injection will be sourced from industrial emitters in the area. The emitters will be responsible for the capture and compression of the CO_2. Emitters will be required to meet contractual requirements for impurity and contaminants limits as well as pressure and temperature requirements. Modeling for the established CO_2 composition was done to ensure compatibility with metallurgies in the system, consistent and manageable physical properties, and injectability. Continuous monitoring of the injectant composition and physical properties will be done in multiple parts of the system.

Chemical and Physical Characteristics

Below is a description of the required composition and characteristics of the CO_2 that will be received from emitters to be transported and injected. The CO_2 will be gathered in the dense phase where it behaves like a liquid. This allows for more efficient transport. The physical and chemical characteristics of the injection stream are projected to be a Claimed as PBI
Claimed as PBI

Daily Rate and Volume and/or Mass and Total Anticipated Volume and/or Mass of the CO_2 Volume

Claimed as PBI

Pressure and Temperature of CO_2 Delivered to the Storage Site

The facility system will be designed to boost the CO_2 at the onshore Central Gathering Facility to meet injection pressure requirements at the wells. Claimed as PBI

Claimed as PBI

5.2.2 Well Design

Maximum Wellhead Injection Pressure

The operating injection pressure will depend on the reservoir pressure, the properties of the injected fluid, the wellbore friction, and the injection rate. OLGA™, a dynamic multiphase flow simulator modeling software package, was used to determine the pressure and temperature profiles for CO_2 injection. OLGA™ has PVT correlations that have been validated for CO_2 injection with a wide range of impurities.

Claimed as PBI

The maximum annulus pressure will meet the maximum injection pressure (MAIP) as required by 40 CFR 146.88(c).

To demonstrate mechanical integrity, the cemented injection casing and tubing and packer will be pressure tested to a pressure equal or greater than the estimated pressures during Well Construction. Once injection commences, the tubing and packer annulus will be tested following the monitoring and testing plans criteria.

Claimed as PBI

Casing and Tubing Program

The Casing and tubing program is designed to meet the well lifecycle conditions from installation through injection and abandonment. The specifications listed in **Table 5-1** are sufficient to meet the 40 CFR 146.86(b)(1)(iv) and to allow operating at the maximum calculated bottom hole pressures.

Claimed as PBI

Injection Liner and Long String (Injection Casing)

Claimed as PBI

Claimed as PBI

Cementing Program

The Cementing Program is designed to meet the well lifecycle conditions. Casing strings will be cemented with industry standard Class H cement with CO_2 resistant additives planned for cement located across the injection interval as demonstrated in each wellbore schematic. Centralizers will be placed throughout the casing string to increase likelihood of full cement coverage around casing. The cement installation will be completed leveraging inner string cement operations for the surface casing and conventional cementing practices for all remaining casing strings with cement planned to be brought to surface for all casing strings, except the liner, which will have cement brought to the top of the liner hanger. Claimed as PBI

Claimed as PBI

Tubing

The Claimed as PBI selected delivers the injection volumes necessary to meet the design requirements. The tubing is designed to handle the full injection lifecycle of pressure, temperature, and resultant stress changes. Claimed as PBI

Claimed as PBI

Claimed as PBI

Claimed as PBI

Packer

The injection packer is designed to anchor and isolate the casing annulus from the injection stream and reservoir. The packer will withstand the full injection lifecycle of pressure, temperature and stress change to meet or exceed industry design and materials standards. The injection packer will be set in cemented, corrosion-resistant casing at or below the confinement layer. This depth will allow for the annual MIT inspections across the Injection interval. The packer bore will be similar to the tubing size to accommodate various logging tools for injection monitoring and mechanical integrity. The packer will be tubing retrievable to allow for future well activities including workovers, interventions, or MIT testing, as necessary. The packer will adhere to API 11D1 guidelines and requirements. **Table 5-2** highlights the anticipated packer ratings that are similar across multiple suppliers.

Annular Fluid

The annular fluid will fill the space between the Claimed as PBI The annular fluid density will impose provide a hydrostatic pressure to meet or exceed the initial reservoir pressure. Surface pressure will be added to annular system to meet or exceed the tubing injection pressures to ensure integrity of the tubing and packer system.

The treated annulus fluid will be a brine solution consisting of fresh water, salt, and corrosion inhibitors. The fluids will be tested to confirm compatibility with reservoir and injection fluids as well as casing and tubing materials. Claimed as PBI Claimed as PBI .

Wellhead

Figure 5-1 describes the proposed wellhead and tree configuration. The components will follow the API Spec 6A – Specification for Wellhead and Tree Equipment. Claimed as PBI Claimed as PBI The design will vary depending on supplier selection process.

The wellhead and tree will be designed for compatibility with the injection fluid (CO_2) to minimize corrosion and pressure rated to meet full life cycle well designs. Flow wetted components that contact CO_2 will be made of corrosion-resistant alloy. The non-flow wetted components will be comprised of carbon steel material.

Well Openings to Formation

The injection wells will connect through the casing to the defined injection interval by utilizing perforations to adequately establish injection rate requirements. Claimed as PBI Claimed as PBI The final perforation interval selection will be confirmed after the drilling and evaluation phases of Well Construction. The perforating technique will be executed using tubing conveyed or wireline guns. Perforation debris clean-up techniques, such as underbalance perforating, may be used in conjunction with the pre-operational testing 40 CFR 146.87 (e) to ensure injectivity requirements.

Schematic of the Subsurface Construction Details of the Example Well(s) – W1

A schematic of the proposed injection well construction is provided as **Figure 5-2**.


Claimed as PBI

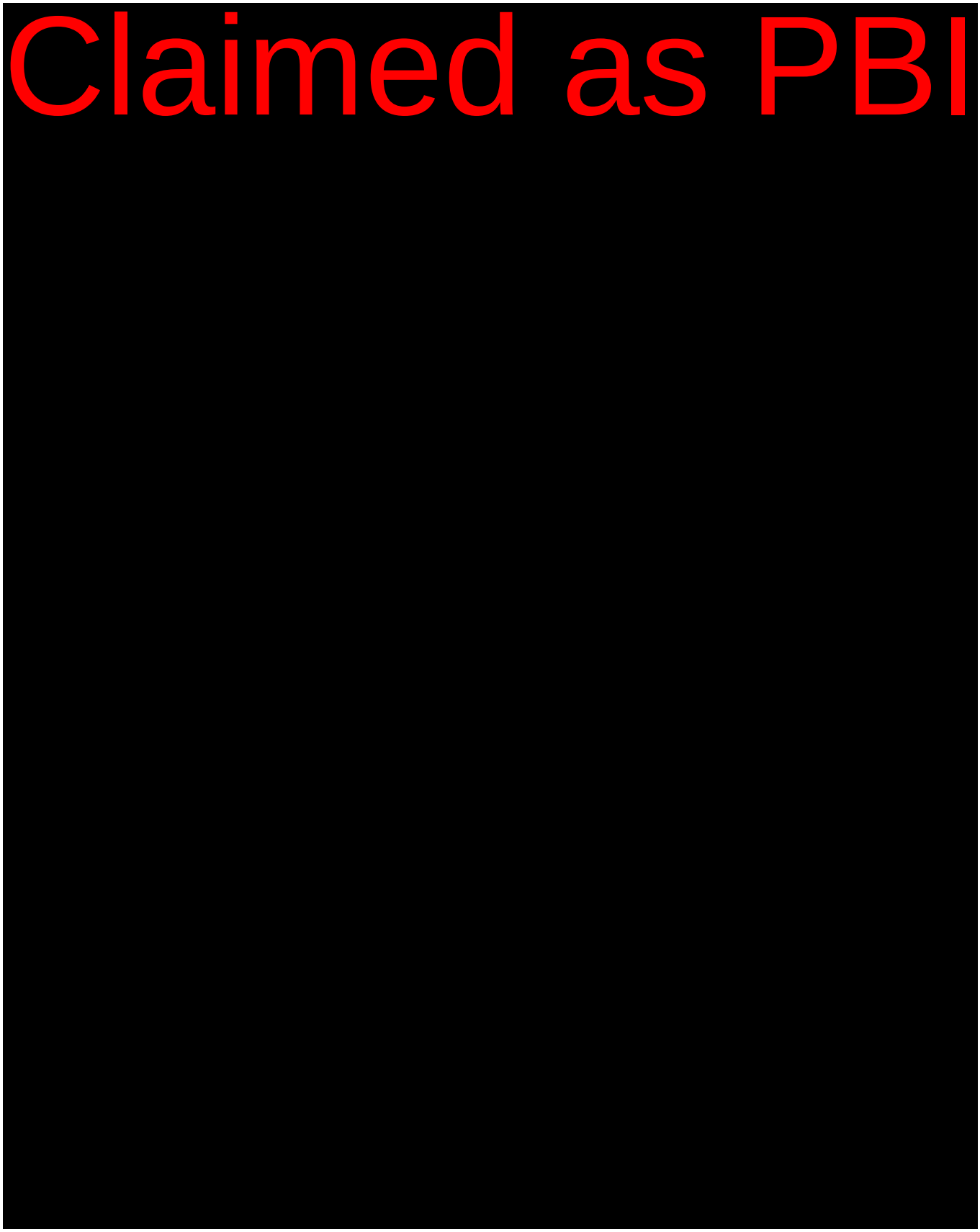
Claimed as PBI

6 PRE-OPERATIONAL LOGGING AND TESTING

A Pre-Operational Logging and Testing Plan was prepared per the requirements of 40 CFR 146.82(a)(8) and 146.87 as part of this application. The plan addresses pre-injection period testing to be conducted on the Claimed as PBI Claimed as PBI The SL20220050 M1 stratigraphic characterization well (API 427083039000) will be converted to a monitoring well for BBE-P1.

The Pre-Operational Logging and Testing Plan associated tables and figures have been uploaded to the GSDT in support of this application.

Pre-Operational Logging and Testing GSDT Submissions
GSDT Module: Pre-Operational Logging and Testing ***Tab(s):*** Welcome tab Please use the checkbox(es) to verify the following information was submitted to the GSDT: ☒ Proposed pre-operational testing program ***[40 CFR 146.82(a)(8) and 146.87]***

7 WELL OPERATION

Well Operation procedures for BBE are provided below, meeting the requirements in 40 CFR 146.82(a)(7) and (10) and 40 CFR 146.88.

7.1.1 Operational Procedures [40 CFR 146.82(a)(10)]

The Operator performed studies to estimate the operational procedures and pressure limits (**Table 7-1**). The studies include regional geomechanical evaluation to assess critical fracture pressure, subsurface reservoir modeling, and injection pressure modeling with CO_2 phase behavior. These values will be finalized and confirmed after construction of the injection wells (Section 2.5).

Claimed as PBI

Additional details regarding fracture pressure and injection pressure are provided in the AOR and Corrective Action document Section 3.2.

Maximum Wellhead Injection Pressures are referenced in Section 5.2.2.


Claimed as PBI

7.1.2 Proposed Carbon Dioxide Stream [40 CFR 146.82(a)(7)(iii) and (iv)]

CO_2 for injection will be sourced from industrial emitters in the area. The emitters will be responsible for the capture and compression of the CO_2. Claimed as PBI [redacted] Claimed as PBI [redacted] The CO_2 stream will be continuously monitored using an online analyzer downstream of the equipment at the Central Gathering Facility. Physical samples of the gas will also be collected and sent to a laboratory. These characteristics will be monitored quarterly to meet the requirements of 40 CFR 146.90(a) [Testing and Monitoring Plan, Section 7.3].

8 TESTING AND MONITORING

A Testing and Monitoring Plan was prepared per the requirements of 40 CFR 146.90 as part of this application. Claimed as PBI [redacted] Claimed as PBI [redacted] The Testing and Monitoring Plan will assess 1) the location of the CO_2 front, 2) the region of highest elevated reservoir pressure (near injectors), and 3) the containment of CO_2 below the confining zone. The technologies and techniques for this monitoring plan were selected based on a site-specific focus area as determined by the site characterization, reservoir modeling and simulation, and AOR sensitivity analysis.

In addition to demonstrating that the wells are operating as planned and the CO_2 saturation and pressure front are moving as predicted, the monitoring data will be used to validate and adjust the geological models used to predict the distribution of the CO_2 within the injection zone to support AOR reevaluations and a non-endangerment demonstration.

The Testing and Monitoring Plan, associated tables, figures, and the Quality Assurance and Surveillance Plan have been uploaded to the GSDT in support of this application.

Testing and Monitoring GSDT Submissions
GSDT Module: Project Plan Submissions ***Tab(s):*** Testing and Monitoring tab Please use the checkbox(es) to verify the following information was submitted to the GSDT: ☒ Testing and Monitoring Plan ***[40 CFR 146.82(a)(15) and 146.90]***

9 INJECTION WELL PLUGGING

Injection Well Plugging Plans were prepared per the requirements in 40 CFR 146.92 [40 CFR 146.82 (a)(16) and 146.92(b)] as part of this application. The Injection Well Plugging plan includes planned mechanical integrity testing activities, proposed plugging details and procedures, and a proposed abandonment schematic.

The costs associated with the proposed Class VI well closures are provided in the Financial Assurance Module, per 40 CFR 146.85.

The Injection Well Plugging Plan, associated tables, figures, and appendices have been uploaded to the GSDT in support of this application.

Injection Well Plugging GSDT Submissions
GSDT Module: Project Plan Submissions ***Tab(s):*** Injection Well Plugging tab Please use the checkbox(es) to verify the following information was submitted to the GSDT: ☒ Injection Well Plugging Plan ***[40 CFR 146.82(a)(16) and 146.92(b)]***

10 POST-INJECTION SITE CARE (PISC) AND SITE CLOSURE

A PISC and Site Closure Plan was prepared per the requirements in 40 CFR 146.82 (a) (17) – (18) and 40 CFR 146.93 as part of this application. The PISC and Site Closure Plan describes how the Operator will monitor ground water quality and track the position of the CO_2 saturation and pressure fronts for 50 years unless an alternative timeframe duration is discussed and approved by UIC Program Director following cessation of injection pursuant to 40 CFR 146.93(b). Following approval for site closure, the Operator will plug monitoring wells, restore the site to its original condition, and submit a site closure report and associated documentation.

An Alternative PISC Timeframe Demonstration is not provided as part of this application at this time.

The PISC and Site Closure Plan with associated tables and figures have been uploaded to the GSDT in support of this application.

PISC and Site Closure GSDT Submissions
GSDT Module: Project Plan Submissions ***Tab(s):*** PISC and Site Closure tab Please use the checkbox(es) to verify the following information was submitted to the GSDT: ☒ PISC and Site Closure Plan ***[40 CFR 146.82(a)(17) and 146.93(a)]***
GSDT Module: Alternative PISC Timeframe Demonstration ***Tab(s):*** All tabs (only if an alternative PISC timeframe is requested) Please use the checkbox(es) to verify the following information was submitted to the GSDT: ☐ Alternative PISC timeframe demonstration ***[40 CFR 146.82(a)(18) and 146.93(c)]***

11 EMERGENCY AND REMEDIAL RESPONSE

An Emergency and Remedial Response Plan was prepared per the requirements in 40 CFR 146.82 (a) (19) and 40 CFR 146.94 as part of this application. This plan has been uploaded to the GSDT in support of this application.

Emergency and Remedial Response GSDT Submissions

GSDT Module: Project Plan Submissions
Tab(s): Emergency and Remedial Response tab

Please use the checkbox(es) to verify the following information was submitted to the GSDT:
☒ Emergency and Remedial Response Plan ***[40 CFR 146.82(a)(19) and 146.94(a)]***

12 INJECTION DEPTH WAIVER AND AQUIFER EXEMPTION EXPANSION

Neither an injection depth waiver nor aquifer exemption expansion will be requested as part of this permit application.

Injection Depth Waiver and Aquifer Exemption Expansion GSDT Submissions

GSDT Module: Injection Depth Waivers and Aquifer Exemption Expansions
stite

Please use the checkbox(es) to verify the following information was submitted to the GSDT:
☐ Injection Depth Waiver supplemental report ***[40 CFR 146.82(d) and 146.95(a)]***
☐ Aquifer exemption expansion request and data ***[40 CFR 146.4(d) and 144.7(d)]***

13 ADDITIONAL INFORMATION

13.1 Community Engagement

The Operator identified communities through assessments including utilization of the EPA EJScreen Tool. The Operator has been actively engaging with the nearby communities.

The Beaumont and Port Arthur, Texas areas were identified as having greater than 80% of the population, compared to United States averages, having a community-level vulnerability based on the supplemental demographic index.

The Operator's community outreach and investments are aimed at strengthening nearby communities and enriching lives, at the same time fostering valuable collaborations by:

- Supporting well-run organizations and investments that align with project drivers and focus areas that meaningfully address nearby community needs.
- Maintaining and fostering relationships that position the Operator as a well-respected industry leader and partner of choice in the local community.
- Establishing strong external communications.

Community outreach efforts for BBE include social investments to the Southeast Texas Food Bank, which serves eight counties and distributes to approximately 130 nonprofit agencies within these counties. Their partner agencies offer approximately 90,000 meals to people in need each month. Additional community non-profits that BBE supports include the Port Arthur Education Foundation and the Winnie, Texas Marsh Fest which directly contributes to scholarships for students in Jefferson and Chambers County. The Operator supports four local Chamber of Commerce organizations. The Chamber serves as a unified voice and economic catalyst to ignite partnerships for the business community, local governments, legislative representatives, that will positively impact the development of the project communities and the region. BBE team members have also volunteered at local community events such as the Rotary Club of Port Arthur's service projects, Earth Day's Street Clean Up, and Port Arthur Independent School District student interviews.

13.2 Acronyms

°F	Degree Fahrenheit
Claimed as PBI	
AOR	Area of Review
AP	Artificial Penetration
BBE	Bayou Bend East SL20220050
BBE-P1	Bayou Bend East SL20220050 – Phase 1
BOEM	Bureau of Ocean Energy Management
CCS	carbon transport and sequestration
Claimed as PBI	
CO_2	carbon dioxide
EoD	Environment of Deposition
FPP	fracture propagation pressure
ft	feet
Fm	Formation
GoM	Gulf of Mexico
GR	gamma ray
Claimed as PBI	
Hz	Hertz
LOT	Leak-off test
Claimed as PBI	
m.y.	million years
Claimed as PBI	
MAIP	maximum allowable injection pressure
MD	measured depth
MDT	modular formation dynamics tester
MEM	Mechanical Earth Model
MFS	maximum flooding surface
mg/L	milligram per liter
MIT	Mechanical integrity test
Claimed as PBI	

MMT	Million metric tonnes
MTA	million metric tonnes per annum
N_2	nitrogen
PISC	Post-injection Site Care
ppg	pounds per gallon
ppm	parts per million
psia	pound per square inch absolute
psi/ft	pounds per square inch per foot
RES	Deep resistivity
Claimed as PBI	
S_{hmax}	maximum horizontal stress
S_{hmin}	minimum horizontal stress
Claimed as PBI	
SGR	shale gouge ratio
SP	Spontaneous potential
SRT	step-rate test
Claimed as PBI	
t/d	tonnes per day
TD	total depth
TDS	total dissolved solids
Claimed as PBI	
TST	true stratigraphic thickness
TVDSS	true vertical depth below sea level
UIC	Underground Injection Control
Claimed as PBI	
USDW	underground source of drinking water
USGS	United States Geologic Survey
Vclay	Clay volume
Vshale	Shale volume

13.3 References

Claimed as PBI

API 5CT, 2011. American Petroleum Institute Specification for Casing and Tubing: ISO 11960:2011 Petroleum and natural gas industries — Steel pipes for use as casing or tubing for wells. 9th edition. June 2011.

Baker, Ernest T. Stratigraphic and hydrogeologic framework of part of the coastal plain of Texas. Vol. 77. No. 712. Texas department of water resources, 1979.

Berggren, W. A., Hilgen, F. J., Langereis, C. G., Kent, D. V., Obradovich, J. D. Raffi, I, Raymo, M. E., Shackleton; N. J., Late Neogene chronology: New perspectives in high-resolution stratigraphy. GSA Bulletin 1995; 107 (11): 1272–1287. doi: https://doi.org/10.1130/0016-7606(1995)107<1272:LNCNPI>2.3.CO;2.

Bruce, C.H., 1972, Pressured shale and related deformation: a mechanism for development of regional contemporaneous faults: Gulf Coast Association, Geological Society Transactions, v. 22, p. 23-31.

Bureau of Economic Geology, 2021. Texas Seismological Network and Seismology Research (TexNet). https://www.beg.utexas.edu/texnet-cisr/texnet/earthquake-catalog. Referenced April 2024.

Bureau of Ocean Energy Management (BOEM), 2019. Atlas of Gulf of Mexico Gas and Oil Sands Data, U.S. Department of the Interior, Atlas of Gulf of Mexico Gas and Oil Sands Data (boem.gov), accessed June 2023

Byerlee, James. "Friction of rocks." Rock friction and earthquake prediction (1978): 615-626.

Cerveny, K., Davies, R., Dudley, G., Fox, R., Kaufman, P., Knipe, R., and Krantz, B., 2005, Reducing uncertainty with fault-seal analysis: Oilfield Review, Winter 2004/2005p. 38-51.

Childs, C., Manzocchi, T., Walsh, J. J., Bonson, C., Nicol, A., and Schöpfer, M., 2009, A geometric model of fault zone and fault rock thickness variations: Journal of Structural Geology, v. 31, p. 117-127.

Chowdhury, A.H. and Turco, M.J., 2006. Geology of the Gulf coast aquifer, Texas: Chapter 2, Texas Water Development Board Report, 365, p. 23-50. TWDB 365 chp2 (texas.gov)

Chowdhury, A.H., Boghici, R., and Hopkins, J., 2006. Geology of the Gulf coast aquifer, Texas: Chapter 5, Texas Water Development Board Report, 365 ch05-GC_Chemistry.pdf

Cooper, H.H., 1964. A hypothesis concerning the dynamic balance of fresh water and salt water in a coastal aquifer. In: H.H. Cooper, F.A. Kohout, H.R. Henry and R.E. Glover (Editors), Sea Water in Coastal Aquifers, U.S. Geol. Surv. Water-supply Pap. 1613-C: 1-12.

Curray, J.R., 1960, Sediments and history of Holocene transgression, continental shelf, northwest Gulf of Mexico: American Association of Petroleum Geologists Symposium, Project 51, p. 1951-1958.

Ewing, T. E., 1991, Structural framework, in Salvador, A. ed., The Gulf of Mexico Basin, The Geology of North America, Geological Society of America, Boulder, CO, v. J, pp. 31–52.

Galloway, W. E., Henry, C. D., and Smith, G. E., 1982, Depositional framework, hydrostratigraphy, and uranium mineralization of the Oakville Sandstone (Miocene), Texas Coastal Plain: The University of Texas at Austin, Bureau of Economic Geology Report of Investigations No.113, 51 p.

Galloway, W. E., Jirik, L. A., Morton, R. A., and DuBar, J. R., 1986, Lower Miocene (Fleming) Depositional Episode of the Texas Coastal Plain and Continental Shelf: Structural Framework, Facies, and Hydrocarbon Resources: The University of Texas at Austin, Bureau of Economic Geology, Report of Investigations No. 150, 50 p.

Galloway, William E. "Genetic stratigraphic sequences in basin analysis II: application to northwest Gulf of Mexico Cenozoic basin." *AAPG bulletin* 73.2 (1989): 143-154.

Galloway, W.E., Ganey-Curry, P.E., Li, X., and Buffler, R.T., 2000, Cenozoic depositional history of the Gulf of Mexico Basin: American Association of Petroleum Geologists Bulletin, v. 84, n. 11, p. 1743-1774.

Galloway, William E. "Gulf of Mexico Basin depositional record of Cenozoic North American drainage basin evolution." *Fluvial sedimentology VII* (2005): 409-423.

Galloway, William E. "Depositional evolution of the Gulf of Mexico sedimentary basin." *Sedimentary basins of the world* 5 (2008): 505-549.

Galloway, W.E., Whiteaker, T.L., and Ganey-Curry, P., 2011, History of Cenozoic North American drainage basin evolution, sediment yield, and accumulation in the Gulf of Mexico basin: Geosphere, v. 7, n.4, p.938-973, https://doi.org/10.1130/GES00647.1

Hall, D. J., T. D. Cavanaugh, J. S. Watkins, and K. J. McMillen, 1982, The rotational origin of the Gulf of Mexico based on regional gravity data, in J. S. Watkins and C. L. Drake, eds., Studies in continental margin geology: AAPG Memoir 34, p. 115 –126.

Haq, Bilal U., J. A. N. Hardenbol, and Peter R. Vail. "Chronology of fluctuating sea levels since the Triassic." Science 235.4793 (1987): 1156-1167.

Jones, Paul H., 1969. "Hydrodynamics of Geopressure in the Northern Gulf of Mexico Basin." *J Pet Technol* 21 (1969) : 803–810. doi: https://doi.org/10.2118/2207-PA

Khodaverdian, M., et al. "Injectivity and fracturing in unconsolidated sand reservoirs: Waterflooding case study, offshore Nigeria." ARMA US Rock Mechanics/Geomechanics Symposium. ARMA, 2010.

Kreitler, Charles W., M. Saleem Akhter, and Andrew CA Donnelly. *Hydrologic-Hydrochemical Characterization of Texas Gulf Coast Saline Formations Used for Deep-Well Injection of Chemical Wastes*. Robert S. Kerr Environmental Research Laboratory, Office of Research and Development, US Environmental Protection Agency, 1988.

Labourdette, Richard, Philippe Crumeyrolle, and Eduard Remacha. "Characterization of dynamic flow patterns in turbidite reservoirs using 3D outcrop analogues: Example of the Eocene Morillo turbidite system (south-central Pyrenees, Spain)." *Marine and Petroleum Geology* 25.3 (2008): 255-270.

Lundstern, Jens-Erik, and Mark D. Zoback. "State of stress in Texas: Implications for induced seismicity." Geophysical Research Letters 43.19 (2016): 10-208.

Manzocchi, T., Walsh, J.J., Nell, P., and Yielding, G., 1999, Fault transmissibility multipliers for flow simulation models: Petroleum Geoscience, v. 5, p. 53-63.

MarineTraffic.com, 2024. Marine Traffic: Global Ship Tracking. MarineTraffic.com Last visited 2024-04-24.

Martinius, Allard W., et al. "Geologic reservoir characterization and evaluation of the Petrocedeno field, early Miocene Oficina Formation, Orinoco heavy oil belt, Venezuela." (2013): 103-131.

McCleskey, R. Blaine; Cravotta, Charles A.; Miller, Matthew P.; Tillman, Fred; Stackelberg, Paul. Knierim, Katherine J.; Wise. Daniel R., 2023. Salinity and total dissolved solids measurements for natural waters: An overview and a new salinity method based on specific conductance and water type. Applied Geochemistry, Volume 154, 2023.

Naruk, S. J., et al., 2002. "Common Characteristics of Proven Sealing and Leaking Faults." AAPG Hedberg Research Conference: December 1-5, 2002, Barossa Valley, South Australia.

Nicholson, Andrew Joseph. "Empirical analysis of fault seal capacity for CO_2 sequestration, Lower Miocene, Texas Gulf Coast." (2012).

Olariu, M.I., DeAngeleo, M., Dunlap, D., and Treviño, R.H., 2019, High frequency (4^{th} order) sequence stratigraphy of early Miocene deltaic shorelines, offshore Texas and Louisiana: Marine and Petroleum Geology, v. 110, p. 575-586, doi.org/10.1016/j.marpetgeo.2019.07.040.

O'Neill, M.W., and Van Siclen, D.C., 1984, Activation of Gulf Coast faults by depressurizing aquifers and an engineering approach to siting structures along their traces: Bulletin of the Association of Engineering Geologists, v. 21, p. 73-87.

Occupational Safety and Health Administration (OSHA), 2023. Standard Industrial Classification (SIC) System Search. https://www.osha.gov/data/sic-search. November 8, 2023.

Qu, Feifei, et al. "Identify and monitor growth faulting using InSAR over northern Greater Houston, Texas, USA." Remote sensing 11.12 (2019): 1498.

Pitman, J.K., 2011, Reservoirs and petroleum systems of the Gulf Coast: American Association of Petroleum Geologists, Datapages GIS Open Files, http://www.datapages.com/AssociatedWebsites/GISOpenFiles/ReservoirsandPetroleumSystemsoftheGu lfCoast.aspx. 2024-04-23.

Posamentier, H. W., and G. P. Allen. "Siliciclastic sequence stratigraphic patterns in foreland, ramp-type basins." *Geology* 21.5 (1993): 455-458.

Rowan, M. G., 1995, Structural styles and evolution of allochthonous salt, central Louisiana outer shelf and upper slope, in Jackson, M. P. A., Roberts, D. G., and Snelson, S. eds., Salt tectonics: a global perspective, American Association of Petroleum Geologists, Tulsa, OK, pp. 199–228.

Salvador, A., 1987. Late Triassic-Jurassic paleogeography and origin of the Gulf of Mexico Basin. Am. Assoc. Pet. Geol. Bull., 71: 419-451. Seni, S.J. and Jackson, M.P.A., 1983. Evolution of salt

Silva, Josimar A; Saló-Salgado, Lluís; Patterson, Joseph; Dasari, Ganeswara; Juanes, Ruben. 2023.. "Assessing the viability of CO_2 storage in offshore formations of the Gulf of Mexico at a scale relevant for climate-change mitigation." International Journal of Greenhouse Gas Control 126 (2023): 103884.

Snee, Jens-Erik Lund. 2020. "State of stress in North America: Seismicity, tectonics, and unconventional energy development". Stanford University, 2020.

SONRIS- Strategic Online Natural Resources Information System. Louisiana Department of Energy and Natural Resources. https://www.sonris.com/. last visited 2024/04/24.

Sperrevik, Susanne; Gillespie, Paul A.; Fisher, Quentin J.; Halvorsen, Trond; Knipe, Rob J., 2002. . "Empirical estimation of fault rock properties." *Norwegian Petroleum Society Special Publications*. Vol. 11. Elsevier, 2002. 109-125.

Stevenson, Donald A. and Agnew, James D., 1998. "Lake Charles, Louisiana, earthquake of 16 October 1983." Bulletin of the Seismological Society of America 78.4 (1988): 1463-1474.

Texas Historical Commision, 2023. *Tribal Contacts*. 09 November 2023. https://www.thc.texas.gov/project-review/tribal-consultation-guidelines/tribal-contacts. last visited 2024/04/24.

Texas Water Development Board database, 2024. Groundwater Database Reports and Downloads. https://www.twdb.texas.gov/groundwater/data/gwdbrpt.asp. Last visited 2024/04/24.

Treviño, R., and Meckel, T. (2017). *Geological CO_2 Sequestration Atlas of Miocene Strata, Offshore Texas State Waters.* Austin, Texas: The University of Texas at Austin: Bureau of Economic Geology. 74p.

USEPA, 2013. *Underground Injection Control (UIC) Program VI Well Area of Review Evaluation and Corrective Guidance.* Ground Water, Report No. EPA 816-R-13-005.

US Geological Survey, 2024. Earthquake Hazards Program. https://www.usgs.gov/programs/earthquake-hazards. Referenced April 2024.

Van Siclen, D.C., 1967, The Houston fault problem: American Association of Petroluem Geologists, Proceedings of the Third Annual Meeting: Texas Section, American Institute of Professional Geologists, p. 9-31.

Vrolijk, P.J., Urai, J.L., and Kettermann, M., 2016, Clay smear: review of mechanisms and applications: Journal of Structural Geology, v. 86, p. 95-152, doi:/10.1016/j.jsg.2015.09.006

Wallace, K. J., Meckel, T. A., Carr, D. L., Treviño, R. H., and Yang, C., 2014, Regional CO_2 sequestration capacity assessment for the coastal and offshore Texas Miocene interval: Greenhouse Gases: Science and Technology, v. 4, no. 1, p. 53–65.

Watkins, J. S., MacRae, G., and Simmons, G. R., 1995, Bipolar simple-shear rifting responsible for distribution of mega-salt basins in Gulf of Mexico, in Gulf Coast Section SEPM 16th Annual Research Conference, pp. 297–305.

Weber, K. J. "Petroleum geology of the Niger Delta." *Proceed. World Petrol. Congr.* 2 (1975): 209-221.

Williamson, A. K. and Grubb, H. F., 2001, Groundwater flow in the Gulf Coast aquifer systems, Regional aquifer system analysis—Gulf Coastal Plain, U.S. Geological Survey Professional Paper 1416-F, 173 p. https://pubs.usgs.gov/pp/1416f/report.pdf

Winker, C., D., and R .T. Buffler, 1988, Paleogeographic evolution of the early deep-water Gulf of Mexico and its margins, Jurassic to middle Cretaceous (Comanchean): AAPG Bulletin, vol. 72, p. 318–346.

Witrock, R. B., L. D. Nixon, P. J. Post, and K. M. Ross, 2003, Biostratigraphic chart of the Gulf of Mexico Offshore Region, Jurassic to Quaternary, U. S. Department of the Interior, Bureau of ocean Energy Management, New Orleans, Louisiana.

Winker, Charles D., and Richard T. Buffler. "Paleogeographic evolution of early deep-water Gulf of Mexico and margins, Jurassic to Middle Cretaceous (Comanchean)." AAPG bulletin 72.3 (1988): 318-346.

Yielding, G., Freeman, B., and Needham, D.T., 1997, Quantitative fault seal prediction: American Association of Petroleum Geologists Bulletin, v. 81, n. 6, p. 897-917.

Young, S., Ewing, T., Hamlin, S., Baker, E., Lupton, D., (2012). Final Report Updating the Hydrogeologic Framework for the Northern Portion of the Gulf Coast Aquifer. https://www.twdb.texas.gov/publications/reports/contracted_reports/doc/1004831113_GulfCoast.pdf

Zhang, Liwei, et al. "Geochemistry in geologic CO2 utilization and storage: A brief review." *Advances in Geo-Energy Research* 3.3 (2019): 304-313.

Appendices


Claimed as PBI

Claimed as PBI

SEPARATE FILE

Revision number: 0
Plan revision date: June 2024

Claimed as PBI

SEPARATE FILE